DOE Contract Number DE-AI105-94ER61 877

FINAL REPORT

ATMOSPHERIC CHEMISTRY PROGRAM

GLOBAL 3-D MODELING OF ATMOSPHERIC OZONE IN THE FREE TROPOSPHERE AND THE STRATOSPHERE WITH EMPHASIS ON MIDLATITUDE REGIONS

Guy Brasseur, Xuexi Tie, and Stacy Walters

National Center for Atmospheric Research

P. O. BOX 3000, Boulder, CO 80307-3000

Office of Energy Research

Office of Health and Environmental Research

Environmental Science Division

DISCLAIMER

TABLE OF CONTENTS

ABSTRACT

We have used several global chemical/transport models (1) to study the contribution of various physical, chemical, and dynamical processes to the budget of mid-latitude ozone in the stratosphere and troposphere; (2) to analyze the potential mechanisms which are responsible for the observed ozone perturbations at mid-latitudes of the lower stratosphere and in the upper troposphere; (3) to calculate potential changes in atmospheric ozone response to anthropogenic changes (e.g., emission of industrially manufactured CFCs, CO, and NOx) and to natural perturbations (e.g., volcanic eruptions and biomass burning); and (4) to estimate the impact of these changes on the radiative forcing to the climate system and on the level of UV-B radiation at the surface.

1. INTRODUCTION

Total ozone has been continuously monitored over the last decade, both by ground-based and space-borne instrumentation. The analysis of the data reveals that, while the ozone abundance has been fairly constant in the tropics, it has decreased dramatically at high latitudes, particularly in the southern hemisphere. Observations have also revealed the existence of a significant downward trend in total ozone at mid-latitudes, (typically 4% /decade on the average and as much 6%/decade in winter at 45°N). This trend is not well reproduced by current models, which suggests that its cause is not yet completely understood. Proposed hypotheses to explain the reduction in mid-latitude stratospheric ozone include (1) the possible dilution of airmasses processed by polar stratospheric clouds inside the polar vortex during winter or (2) the destruction of ozone via heterogeneous reactions on the surface of aerosol particles which are present at all latitudes. The first hypothesis involves the rapid conversion of nitrogen oxides into nitric acid, and of chlorine nitrate and hydrogen chloride into active forms of inorganic chlorine at high latitudes, the transport of processed air through the polar vortex towards lower latitudes and catalytic destruction of ozone in regions where solar radiation is sufficiently intense.

The second hypothesis to explain stratospheric ozone depletion at mid-latitudes involves heterogeneous conversion of nitrogen oxides and chlorine nitrate on the surface of sulfate aerosol particles. Rodriguez et al. (1991) as well as Granier and Brasseur (1992) have shown that the observed ozone trends at mid-latitudes was better reproduced in numerical models when the effects of these aerosols were taken into account. This raises the question of the impact of

large volcanic eruptions on stratospheric ozone, especially at mid-latitudes.

As stratospheric ozone is being depleted at mid-latitudes, ozone concentrations are increasing in the troposphere (northern hemisphere), most probably as a result of human activities. Ozone is produced in the troposphere during daytime when the concentrations of hydrocarbons and nitrogen oxides are sufficiently high, such as in the boundary layer of industrialized regions, while hydrocarbons are produced either naturally by vegetation (e.g., isoprene, terpenes, other VOC's) or anthropologically in urbanized areas. Most studies have focused on the formation of ozone in the planetary boundary layer, but only a few of them have attempted to quantify the components of the ozone budget in the free troposphere. These components include (1) the photochemical formation of ozone, which can be significant near thunderstorm cell where NOx is produced by lightning, (2) the chemical destruction of ozone by HOx radicals, (3) the contribution of ozone and its precursors exported from the "polluted" boundary layers over regions such as the eastern US, Europe, China, Japan, etc., (4) the intrusion of ozone-rich stratospheric air, and (5) the deposition of ozone on the surface. Figure 1 presents a model estimate of the vertical integrated net photochemical production of ozone in the troposphere obtained by the IMAGES model (Muller and Brasseur, 1993). The existence of different regimes, associated with the level of NOx, is clearly visible. The photochemical production of ozone over continents at mid-latitudes is significant in the northern hemisphere. Figure 2, which represents meridional cross section of ozone shows that mid-latitudes are affected not only by photochemical production at low levels, but also, most probably, by stratosphere-troposphere exchanges. The cross tropopause fluxes of ozone may also be perturbed by large volcanic eruptions.

We have used a hierarchy of existing two- and three-dimensional chemical/transport models of the global atmosphere to address key scientific questions related to stratospheric and tropospheric ozone, with emphasis on mid-latitude processes. We have also assessed the potential response of ozone to human perturbations (e.g., emissions of CFCs, NOx, CO, and CH_4), and the impact of the ozone changes on radiative forcing (climate).

2. BRIEF DESCRIPTION OF THE MODELS

Four models have been improved and used:

(1) A two-dimensional chemical-radiative-dynamical model

The model, described in Brasseur et al. (1990), extends from the surface to 85 km, with a vertical resolution of 1 km, and from 85°S to 85°N, with a latitudinal resolution of 5°. Radiation, chemistry and dynamics are treated interactively above the tropopause. A description of the dynamical aspects is given in Brasseur and Hitchman (1987), and Brasseur et al. (1990). Temperature and tracer families are integrated semi-implicitly with a 15 day time step. Zonal winds are diagnosed from thermal wind balance and are used to determine the body forces due to Rossby and gravity waves and corresponding distributions of vertical and meridional eddy diffusivities. The body forces and net heating rates are used to diagnose the residual circulation, hence advection terms for the next time step. The streamfunction solver uses an internal boundary condition at the tropopause which may be tuned to obtain a good "Dobson diagram". It exerts a powerful control on the temperature and on the circulation well into the stratosphere.

The model calculates the distribution of 56 species. It provides the 24-hour average of the concentration of each species, from the surface to 85 km altitude. The rate of the reactions are based on JPL (DeMore et al., 1997). The photodissociation rates are calculated by spectral integration, using the 171 wavelength intervals specified by Ackerman (1972). The solar irradiances are specified according to Brasseur and Simon (1981). The absorption cross-sections are from DeMore et al. (1997). The net adiabatic rate is calculated by using the radiative code of the NCAR community model (CCM1, Kiehl et al., 1987). Parameterization of the heterogeneous processes occurring on the surface of the polar stratospheric clouds (PSCs) are included. For the calculations concerning the effects of sulfate aerosols, we have included the stratospheric aerosol microphysical processes (sulfur cycle, nucleation, condensation, evaporation, coagulation, gravitational sedimentation, and washout) in the model. The aerosol particles are assumed to be spherical liquid droplets. The size distribution of the aerosol particles is represented by 25 discrete bins covering a range of particle radii from 0.01 um to 2.56 um, with particle volume doubling from one bin to the next. The aerosol particles are transported in the same fashion as the gaseous chemicals. The detailed numerical treatment of the microphysical processes in the model is described by Tie et al. (1993). Both background and volcanic aerosol distributions are calculated by using the microphysical model. Two important chemical reactions on the surface of aerosol are included in the model, such as $N_2O_5 + H_2O(A)$ and $ClNO_3 + H_2O(A)$.

(2) *Stratospheric version of three-dimensional off-line chemical-transport model (STARS)*

The STARS (Study of Transport And Chemical Reactions in the Stratosphere) chemical-

transport model is developed at National Center for Atmospheric Research, and the details of the model are described in Brasseur et al. (1997). The model extends from the surface to an approximate altitude of 80 km. The spatial resolution is 2.8 degrees in latitude and 5.6 degrees in longitude, with 44 levels in the vertical (approximately 13 in the troposphere, 25 in the stratosphere, and 6 in the mesosphere). The model includes 46 species with a representation of 154 chemical and photochemical reactions that affect the oxygen, hydrogen, nitrogen, chlorine, and bromine families in the stratosphere. In the present model study, 17 heterogeneous processes occurring on the surface of sulfate aerosol particles and on PSC particles are explicitly included. The chemical reactions are emphasized for stratospheric region (e.g., comprehensive chlorine and bromine chemistries are included in the model) as shown in Tables 1 and 2. The longer chemical lifetime species are transported by advective (Rasch and Williamson, 1991), diffusive (Holtslag and Boville, 1993), and convective (Hack, et al., 1993) processes. The meteorological fields used to drive STARS are taken from a simulation of the general circulation model (GCM) which is the middle atmosphere version of CCM2. Details of the GCM are described by Boville (1995).

(3) *Tropospheric version of three-dimensional off-line chemical-transport model (MOZART)*

MOZART (Model of OZone And Related chemical Tracers) is a three-dimensional (3-D) Chemical-Transport-Model driven by global winds, temperature, humidity, and cloud fields provided by the NCAR Community Climate Model (CCM, version 3) (Hack et al., 1993). A detailed description of chemistry, emission, deposition, and transport is given in Brasseur et al. (1996). The version of the model used in the present study computes the time history of 50

chemical species on the global scale from the surface to the upper stratosphere. In its present configuration, the model is run with a spatial horizontal resolution which is identical to that of the standard CCM3 (triangular truncation at 42 waves or T42) with a corresponding numerical grid of 64 gaussian latitudes and 128 equidistant longitudes (corresponding to a 2.8 degree horizontal resolution). In the vertical, the model uses a hybrid coordinate with 25 levels extending from the surface to 5 mbar. The numerical time-step for both transport and chemistry is 20 minutes, so that the diurnal evolution of chemical species is explicitly represented. MOZART is run "off line" from CCM3, with dynamical variables (e. g. wind components, pressure, temperature, water vapor, convective mass fluxes, diffusion parameters, cloudiness) provided every 3 hours from pre-established history tapes.

The model accounts for surface emissions of chemical compounds (based on the emission inventories of Muller, 1992), advective transport (using the Semi-Lagrangian Transport scheme of Williamson and Rasch, (1994)), convective transport using the formulation of Hack (1994) adopted in CCM2, diffusive exchanges in the boundary layer (based on the parameterization of Holtstag and Boville, 1993). In-cloud wet scavenging uses the formulation of Giorgi and Chameides, (1986). However, for very soluble chemical species (such as HNO_3), the equilibrium time scale between gas phase and aqueous phase in a rain droplet is quite long, so that under-cloud scavenging is included in the wet deposition scheme for HNO_3 following Levine and Schwartz, (1982). Surface dry deposition is simulated according to Muller (1992). The chemical scheme with its 50 species (including CH_4, C_2H_4, C_2H_6, C_3H_6, C_3H_8, C_4H_{10}, isoprene, and terpenes degradation schemes) includes approximately 130 chemical and photochemical reactions, as well as wash-out processes for approximately 10 soluble species.

The chemical reactions are emphasized for tropospheric region (e.g., comprehensive hydrocarbon chemistries are included in the model) as shown in Tables 3 and 4. The heterogeneous conversion of NO_3 and N_2O_5 into HNO_3 on the surface of sulfate aerosols is crudely parameterized as in Muller and Brasseur (1995), using the pre-calculated sulfate concentrations provided by Pham et al. (1995). The NO_x sources represented in this model include the contributions of fossil fuel combustion, biomass burning, soil emissions, lightning and geographically distributed according to the parameterization of Price and Rind, (1992), and aircraft emissions (Albritton, 1993). The model has been used recently to investigate the time evolution and distribution of chemical species in the Pacific Troposphere in conjunction with the measurements collected during the MLOPEX campaigns (Brasseur et al., 1996). An example of the ozone mixing ratio calculated by the model at Mauna Loa is given in Figure 3. Calculated values are compared with observations.

(4) Intermediate model of the global and annual evolution of species (IMAGES)

The IMAGES model represents chemical processes, wet and dry deposition, and surface emissions as in MOZART. The resolution of the model, however, is lower (5x5 degrees in latitude and in longitude) than the resolution of the MOZART model (2.8x2.8 degrees in latitude and in longitude). There are 25 levels, with only 3 of them located in the stratosphere below 50 mb. The model uses a rather long time step (1 day), except during the first 3 days of each month, during which a full diurnal calculation is performed with 1 hour time step. The wind components used to calculate the transport of long-lived species are monthly mean climatological values derived from the analyses of ECMWF. The effect of temporal wind

variability (on time-scales shorter than 1 month) is therefore not explicitly taken into consideration in the advection term of the transport equation. However, large-scale mixing associated with wind variability is parameterized by a diffusion process, which is a function of the observed wind variance. The additional transport components (subgrid processes) which are included in the model are turbulent mixing in the planetary boundary layer and vertical transport associated with convection process. The convection parameterization used in IMAGES is similar to the probabilistic parameterization of Costen et al. (1988). A detailed description, and evaluation of the IMAGES model is given by Muller and Brasseur (1995).

3. ACCOMPLISHMENTS

3.1 Stratospheric ozone

The 2-D model has been used to study the effects of volcanic eruption on stratospheric ozone. Model calculations, summarized in Paper 1 of the Publications suggest that the ozone decrease observed a few years after the eruptions of Mt. Pinatubo and El Chichon may have been unique in the Earth's history, and is directly linked to the emission in the atmosphere of industrially manufactured chlorofluorocarbons. For chlorine loadings typical of the pre-1980 period, the ozone column abundance should have increased after a large volcanic eruption. After 1980, as a result of growth in chlorine loading, the response of ozone became negative in winter at mid- and high latitudes. In the future, the response of ozone is expected to become positive again, if the production of chlorofluorocarbons is sufficiently reduced (see Figure 4).

The model also shows that the inter-annual variability of stratospheric temperature has a strong effect on stratospheric ozone at mid-high latitudes, summarized in Papers 3, 4, 7 and 8 of the Publications. During cold winters, such as the 1992-1993 winter, the stratospheric temperature at mid- and high latitudes in the northern hemisphere was colder than during winter 1991-1992. As a consequence, the rate of heterogeneous conversion from inactive chlorine to active chlorine in sulfate aerosols was faster, and an additional 3 to 5% ozone column decrease occurred during winter 1992-1993 (see Figure 5). Effects of interannual variations of temperature on heterogeneous reactions and stratospheric ozone is studied by the model. Two effects associated with temperature variations are considered: First, the effect on the rate coefficient of heterogeneous reactions occurring at the surface of sulfate aerosols, in particular for the enhanced sulfate aerosols following the eruption of Mount Pinatubo, and second, the effect of temperature interannual variations on the formation of polar stratospheric clouds (PSCs) and the spring Antarctic ozone depletion. The interannual variability of ozone concentration, as affected by both processes, is evaluated. The model results show that during winter 1992-1993, stratospheric temperatures at high latitudes in the northern hemisphere were lower than during winter 1991-1992, leading to a larger rate of heterogeneous conversion of inactive chlorine into active chlorine at northern high latitudes. As a result, ozone reduction due to heterogeneous reactions following the eruption of Mount Pinatubo is enhanced in a colder winter (1992-1993) and reduced in a warmer winter (1991-1992). This result indicates that the enhanced heterogeneous conversion associated with colder temperatures can explain, in part, the large ozone depletion observed by the total ozone mapping spectrometer (TOMS) experiment during winter 1992-1993. The model also shows that during winters 1986 to 1990, the formation rate of PSCs over Antarctica was very variable from year to year, in response to temperature

variability. During the coldest years (1987 and 1989) the surface area of PSCs (a major factor to determine the rate of heterogeneous conversion from inactive chlorine to active chlorine) increases, and the ozone concentration decreases. During the warmest years (1986 and 1988) the results are opposite. The calculated ozone interannual variation is consistent with satellite observations (TOMS), indicating that the interannual variation of the formation of PSCs is likely to play an important role for the interannual variability of the spring Antarctic ozone hole.

The STARS model has been used in several studies which are summarized in Papers 5 and 6 of the Publications. Model calculations suggest that heterogeneous conversion of bromine reservoirs ($BrONO_2$, HOBr) on the surface of aerosol particles in the lower stratosphere has significant effects on the concentration of reactive chlorine species and hydroxyl radicals. Owing to the heterogeneous hydrolysis of $BrONO_2$ and the reaction HOBr+HCl(s) on sulfate aerosols, the increase in total bromine loading from 1960 (12 pptv) to 1990 (21 pptv) has led to an ozone depletion of 2-3% in the lower stratosphere at mid- and high latitudes under post-volcanic conditions. The model is also used to study the formation of the observed springtime "Antarctic ozone hole", and its effect on the ozone concentration at mid-latitudes and in the upper troposphere (see Paper 6). The model results show that a maximum of 40% total ozone depletion occurs in October. After the breakdown of the polar vortex in December, air with depleted ozone is transported to mid-latitudes in the Southern Hemisphere, resulting in a 2-4% ozone decrease at 50°S in December and a 1% decrease in the tropics. Ozone-poor airmasses are also transported to the troposphere, and produce a significant decrease (20-30%) in upper tropospheric ozone (see Figures 6 and 7).

3.2 Ozone exchange between the stratospheric and the troposphere

The STARS model is also used to study the effect of large volcanic eruptions on tropospheric ozone (see Paper 9 off the Publications). The ozone budget is calculated in the northern and southern extratropical lowermost stratosphere and in the tropical upper troposphere during both perturbed and background aerosol conditions. The stratospheric ozone mass flux into the troposphere is highest during the winter months in both hemispheres and higher in the northern hemisphere than in the southern hemisphere. During background aerosol conditions the net modeled stratospheric flux of ozone to the troposphere is 792 Tg/yr. The results suggest that the heterogeneous chemical reactions occurring on the surface of sulfate aerosols in the stratosphere have a significant impact on tropospheric ozone, leading to a possible 15% reduction in the annual global ozone mass transported from the stratosphere to the troposphere after a large volcanic eruption. Most of the reduction in ozone mass flux occurs in the northern hemisphere (see Figure 8).

3.3 Tropospheric ozone

The IMAGES model has been used to study the impact of biomass burning and the development of industrial on tropospheric ozone (see Paper 2 off the Publications). The model is used to study past and future changes in global tropospheric ozone, and their impact on radiative forcing. The results indicate that surface emissions of chemical compounds caused by industrial activities at mid-latitudes in the northern hemisphere and by biomass burning in the tropics, have produced since the middle of the 19th century an increase in the abundance of tropospheric

ozone with an associated reduction in the oxidizing capacity of the atmosphere (methane lifetime enhanced by 1.5 years), and an annually averaged radiative forcing of 0.36 Wm-2. Future changes (1990-2050) in tropospheric ozone associated with population increase and economic development are expected to be largest in the tropics, and especially in South and Southeast Asia (see Figures 9 and 10).

Most recently, we have completed the development of a global three-dimensional model (MOZART) which simulates the distribution of ozone and its precursors in the troposphere and lower stratosphere (see Paper 10 of the Publications). The simulated distributions of ozone and its precursors (methane, non-methane hydrocarbons, carbon monoxide, and nitrogen oxides) are evaluated by comparison with observational data. The model generally reproduces satisfactory the seasonal and geographical variations of species distributions in the troposphere (see Figure 11). A global net photochemical production of ozone in the troposphere of 507 Tg/yr and the surface dry deposition of 898 Tg/yr are derived.

The model is under development to implement aerosol formation, including sulfate, ammonium nitrite, black carbon, and mineral dust aerosols. The purpose of including aerosols into a comprehensive chemical model is to study the interactions between these aerosols and gas-phase chemical species. The interactions between aerosols and photo-oxidants involves heterogeneous reactions on the surface of particles. The impact of heterogeneous reactions on tropospheric ozone will be emphasized.

4. COLLABORATIONS

We have provided global distributions of ozone, OH, H_2O_2, NO_3, and HNO_3 calculated by MOZART to Carmen Benkovitz of Brookhaven National Laboratory. The data will be used in their sulfate aerosol model.

5. REFERNCES

Albritton, D. L., The atmospheric effects of stratospheric aircraft: Interim assessment report of the NASA High-Speed Research Program, *NASA Reference Publication 1333,* 1993

Ackerman, M., in *Hemispheric Models and Related Experiments*, pp 149-159, 1972.

Boville B., Middle atmosphere version of community climate model 2: Annual cycle and interannual variability, *J. Geophys Res., 100*, 9017-9040, 1995.

Brasseur, G., and P.C. Simon, Stratospheric chemical and thermal response to long-term variability in solar UV irradiance *J. Geophys. Res., 86*, 7343-7362, 1981.

Brasseur, G., and M.H. Hitchman, in *Transport processes in the Middle atmosphere,* ed. by G. Visconti and R. Garcia, pp 215-227, D. Reidel, Hingham, Mass., 1987.

Brasseur, G., M.H.Hitchman, S.Walters, M.Dymek, E.Falise, and M.Pirre, An interactive chemical dynamical radiative two-dimensional model of the middle atmosphere, *J. Geophys. Res., 95,* 5639-5655, 1990.

Brasseur, G. P., D. A. Hauglustaine, and S. Walters, Chemical compounds in the remote pacific troposphere: comparison between MLOPEX measurements and Chemical-Transport-Model

calculations, *J. Geophys. Res., 101,* 14795-14813, 1996.

Brasseur, P. G., X. Tie, P. Rasch, and F. Lefevre, A three-dimensional simulation of the Antarctic ozone hole: The impact of anthropogenic chlorine on the lower stratosphere and upper troposphere, *J. Geophys. Res., 102,* 8909-8930, 1997.

Costen R. C., G. M. Tennille, and J. S. Levine, Cloud pumping in a one-dimensional model, *J. Geophys. Res., 93,* 15941-15954, 1988.

DeMore, W.B., S.P. Sander, D.M. Golden, M.J. Molina, R.F. Hampson, M.J. Kurylo, C.J. Howard, and A.R. Ravishankara, *NASA-JPL Publication 90-1,* Jet Propulsion Laboratory, Pasadena, California, 1997.

Giorgi, F., and W. L. Chameides, Rainout lifetimes of highly soluble aerosols and gases as inferred from simulations with a general circulation model, *J. Geophys. Res., 91,* 14,367-14,376, 1986.

Granier, C. and G. Brasseur, Impact of heterogeneous chemistry on model predictions of ozone changes, *J. Geophys. Res., 97,* 18015-18033, 1992.

Hack, J. J., B. A. Boville, B. P. Briegleb, J. T. Kiehl, P. J. Rasch, and D. L. Williamson, Description of the NCAR community climate model (CCM2), *Tech. Note NCAR/TN-382+STR, 108* pop., Natl. Cent. for Atmos. Res., Boulder, Colo., 1993.

Holtslag, A. A. M., and B. A. Boville, Local versus nonlocal boundary-layer diffusion in a global climate model, *J. Clim., 6,* 1825-1842, 1993.

Kiehl, J.T., J. Wolski, B.P. Briegleb, and V. Ramanathan, NCAR *Tech. Note, NCAR/TN-288+IA,* National Center for Atmospheric Research, Boulder, Colorado, 1987.

Muller, J.-F., Geographical distribution and seasonal variation of surface emissions and deposition velocities of atmospheric trace gases, *J. Geophys. Res., 97,* 3787-3804, 1992

Muller, J.-F., and G. Brasseur, IMAGES: a three-dimensional chemical transport model of the global troposphere, *J. Geophys. Res. 100,* 16,445-16,490, 1995.

Rasch, P.J., and D.L. Williamson, The sensitivity of a general circulation model climate to the moisture transport formulation, *J. Geophys. Res., 96,* 13,123-13,137, 1991.

Rodriguez, J. M., M.K.W. Ko, and N. D. Sze, Role of heterogeneous conversion of N2O5 on sulfate aerosols in global ozone losses, Nature, 352, 134-137, 1991.

Pham, M., J.-F. Muller, G. P. Brasseur, C. Granier, and G. Megie, A three-dimensional study of the tropospheric sulfur cycle, *J. Geophys. Res., 100,* 26,061-26,092, 1995

Price, C., and D. Rind, A simple lightning parameterization for calculating global lightning distributions, *J. Geophys. Res., 97,* 9919-9933, 1992.

Tie, X., X. Lin, and G. P. Brasseur, Two-dimensional coupled dynamical/ chemical/ microphysical simulation of global distribution of El Chichon volcanic aerosols, *J. Geophys. Res., 99,* 16779-16792, 1994.

6. TABLES

7. FIGUES

8. APPENDIX: Publications

Reprints removed for separate processing

(1) **Tie, X.**, and **G. P. Brasseur**, The response of stratospheric ozone to volcanic eruptions: Sensitivity to atmospheric chlorine load, *Geophys. Res. lett., 22,* 3035-3038, 1995.

(2) Muller, J.-F., and **G. Brasseur**, IMAGES: a three-dimensional chemical transport model of the global troposphere, *J. Geophys. Res. 100,* 16,445-16,490, 1995.

(3) De Rudder, A, N. Larsen, **X. Tie,** C. Granier, and **G. P. Brasseur,** Model study of polar stratospheric clouds and their effects on stratospheric ozone: Part I- Model description, *J. Geophys. Res.,* 101, 12567-12574, 1996.

(4) **Tie, X., G. P. Brasseur,** C. Granier, A. De Rudder, N. Larsen, Model study of polar stratospheric clouds and their effects on stratospheric ozone: Part II- Model results, *J. Geophys. Res.,* 101, 12575-12584, 1996.

(5) **Tie, X.**, and **G. P. Brasseur,** The importance of heterogeneous bromine chemistry in the lower stratosphere. *Geophys. Res. lett., 23,* 2505-2508, 1996.

(6) **Brasseur, P. G., X. Tie**, P. Rasch, and F. Lefevre, A three-dimensional simulation of the Antarctic ozone hole: The impact of anthropogenic chlorine on the lower stratosphere and upper troposphere, *J. Geophys. Res., 102, 8909-8930,* 1997.

(7) K. Tourpali, **X. Tie,** C. Zerefos, and **G. Brasseur,** Decadel Evolution of total ozone decline: Observations and model results, *J. Geophys. Res., 102,* 23955-23962, 1997.

(8) **Tie, X.**, C. Granier, W. Randel, and **G. Brasseur,** The effects of interannual variation of temperature on heterogeneous reactions and stratospheric ozone, J. Geophys. Res., I02, 23519-23527, 1997.

(9) **Tie, X** and P. Hess, The effects of volcanic eruption on the ozone mass exchange between the stratosphere and the troposphere, *J. Geophys. Res., 102,* 25487-25500, 1997.

(10) **Brasseur, G.P.**, D. A. Hauglustaine, **S. Walters**, P. J. Rasch, J. F. Muller, G. Granier, and **X. X. Tie,** MOZART: A global chemical transport model for ozone and related chemical tracers, Part 1., Model description, In-press, *J. Geophys. Res.,* 1998.

Table 1a. Gas Phase Chemical Reactions Included in the Model and Corresponding Reaction Rates [*DeMore et al.*, 1994]

	Reaction	Rate Coefficient
(1)	$O(^1D) + O_2 \rightarrow 2O_2$	$1.2e-10$
(2)	$O + O + m \rightarrow O_2 + m$	$4.23e-28*am/(T*T)$
(3)	$O + O_2 + m \rightarrow O_3 + m$	$6.0e-34*((300./T)**2.3)*am$
(4)	$O + O_3 \rightarrow O_2 + O_2$	$8.e-12*\exp(-2060./T)$
(5)	$O(^1D) + N_2 \rightarrow O + N_2$	$1.8e-11*\exp(110./T)$
(6)	$O(^1D) + O_2 \rightarrow O + O_2$	$3.2e-11*\exp(70./T)$
(7)	$O(^1D) + N_2 \rightarrow N_2O$	$3.5e-37*((300./T)**0.6)*am$
(8)	$O(^1D) + H_2O \rightarrow 2OH$	$2.2e-10$
(9)	$O(^1D) + CH_4 \rightarrow CH_3 + OH$	$1.4e-10$
(10)	$O(^1D) + CH_4 \rightarrow H_2 + CH_2O$	$1.4e-11$
(11)	$O(^1D) + H_2 \rightarrow OH + H$	$1.0e-10$
(12)	$H + HO_2 \rightarrow OH + OH$	$8.1e-11*0.9$
(13)	$H + HO_2 \rightarrow H_2 + O_2$	$8.1e-11*0.08$
(14)	$H + HO_2 \rightarrow H_2O + O$	$8.1e-11*0.02$
(15)	$H + O_2 + m \rightarrow HO_2 + m$	$5.7e-32*am\ (300./T)**1.6$
(16)	$H + O_3 \rightarrow OH + O_2$	$1.4e-10*\exp(-470./T)$
(17)	$O + OH \rightarrow O_2 + H$	$2.2e-11*\exp(120./T)$
(18)	$OH + O_3 \rightarrow HO_2 + O_2$	$1.6e-12*\exp(-940./T)$
(19)	$HO_2 + O_3 \rightarrow OH + 2O_2$	$1.1e-14*\exp(-500./T)$
(20)	$O + HO_2 \rightarrow OH + O_2$	$3.0e-11*\exp(200./T)$
(21)	$OH + HO_2 \rightarrow H_2O + O_2$	$4.8e-11*\exp(250./T)$
(22)	$OH + H_2 \rightarrow H_2O + H$	$5.5e-12*\exp(-2000./T)$
(23)	$H_2 + O \rightarrow OH + H$	$8.8e-12*\exp(-4200./T)$
(24)	$NO + HO_2 \rightarrow NO_2 + OH$	$3.7e-12*\exp(250./T)$
(25)	$HO_2 + HO_2 \rightarrow H_2O_2 + O_2$	$(2.3e-13*\exp(600./T) + a25)*b25$ $a25 = 1.7e-33*\exp(1000./T)*am$ $b25 = (1. + 1.4e-21*H_2O*\exp(2200./T)$
(26)	$OH + H_2O_2 \rightarrow H_2O + HO_2$	$2.9e-12*\exp(-160./T)$
(27)	$OH + CO \rightarrow CO_2 + H$	$1.5e-13*(1. + .6*am/1013.)$
(28)	$O + H_2O_2 \rightarrow HO_2 + OH$	$1.4e-12*\exp(-2000./T)$
(29)	$OH + OH \rightarrow H_2O + O$	$4.2e-12*\exp(-240./T)$
(30)	$N + NO \rightarrow N_2 + O$	$3.4e-11$
(31)	$N_2O + O(^1D) \rightarrow N_2 + O_2$	$4.9e-11$
(32)	$N_2O + O(^1D) \rightarrow NO + NO$	$6.7e-11$
(33)	$NO_2 + O \rightarrow NO_3 + O_2$	$1.0e-11$
(34)	$NO_2 + OH \rightarrow NO_3 + HO_2$	$2.3e-11$
(35)	$NO_2 + HO_2 \rightarrow HNO_4 + O_2$	$4.1e-12$
(36)	$HNO_4 + m \rightarrow HO_2 + NO_2$	$k_{1(36)}(2.1e-27*\exp(10900./T))*am)$
(37)	$N_2O_5 + m \rightarrow NO_2 + NO_3$	$k_{0(36)}(4.0e-27*\exp(10930./T))*am)$
(38)	$O + NO_2 \rightarrow NO + O_2$	$6.5e-12*\exp(120./T)$
(39)	$O_3 + NO \rightarrow NO_2 + O_2$	$2.e-12*\exp(-1400./T)$
(40)	$N + O_2 \rightarrow NO + O$	$1.5e-11*\exp(-3600./T)$
(41)	$O_3 + NO_2 \rightarrow NO_3 + O_2$	$1.2e-13*\exp(-2450./T)$
(42)	$HNO_3 + OH \rightarrow H_2O + NO_3$	$7.2e-15*\exp(785./T) + aux1/aux2$ $aux1 = 1.9e-33*\exp(725./T)*am$ $aux2 = 1. + aux1/(4.1e-16*\exp(1440./T))$
(43)	$OH + HO_2NO_2 \rightarrow$ products	$1.3e-12*\exp(380./T)$
(44)	$HNO_4 + OH \rightarrow NO_2 + H_2O + O_2$	$1.3e-12*\exp(380./T)$
(45)	$NO_3 + NO \rightarrow NO_2 + NO_2$	$1.5e-11*\exp(170./T)$
(46)	$OH + CH_4 \rightarrow CH_3 + H_2O$	$2.65e-12*\exp(-1880./T)$
(47)	$O(^1D) + CF_3Cl \rightarrow Cl +$ prod.	$2.3e-10$
(48)	$O(^1D) + CF_2Cl_2 \rightarrow 2\,Cl +$ prod.	$1.4e-10$
(49)	$O(^1D) + Cl_2 \rightarrow ClO + Cl$	$2.8e-10$
(50)	$Cl + Cl_2O_2 \rightarrow Cl_2 + Cl + O_2$	$1.0e-10$
(52)	$Cl + NO_3 \rightarrow ClO + NO_2$	$2.6e-11$
(53)	$ClO + NO_3 \rightarrow Cl + NO_2 + O_2$	$4.7e-13$
(54)	$O(^1D) + HCl \rightarrow OH + Cl$	$1.5e-10$
(55)	$OH + CH_3Cl \rightarrow CH_2Cl + H_2O$	$4.0e-12*\exp(-1400./T)$
(56)	$Cl + O_3 \rightarrow ClO + O_2$	$2.9e-11*\exp(-260./T)$
(57)	$ClO + O \rightarrow Cl + O_2$	$3.e-11*\exp(70./T)$
(58)	$ClO + NO \rightarrow NO_2 + Cl$	$6.4e-12*\exp(290./T)$
(59)	$Cl + CH_4 \rightarrow HCl + CH_3$	$1.1e-11*\exp(-1400./T)$
(60)	$Cl + H_2 \rightarrow HCl + H$	$3.7e-11*\exp(-2300./T)$
(61)	$Cl + HO_2 \rightarrow HCl + O_2$	$1.8e-11*\exp(170./T)$
(62)	$ClO + OH \rightarrow Cl + HO_2$	$1.1e-11*\exp(120./T)$
(63)	$OH + HCl \rightarrow H_2O + Cl$	$2.6e-12*\exp(-350./T)$
(64)	$O + ClONO_2 \rightarrow$ products	$2.9e-12*\exp(-800./T)$
(65)	$ClO + HO_2 \rightarrow HOCl + O_2$	$4.8e-13*\exp(700./T)$
(66)	$OH + HOCl \rightarrow H_2O + ClO$	$3.0e-12*\exp(-500./T)$
(67)	$Cl + HOCl \rightarrow OH + Cl_2$	$3.e-12*\exp(-130./T)$
(68)	$OClO + OH \rightarrow HOCl + O_2$	$4.5e-13*\exp(800./T)$
(69)	$Cl + OClO \rightarrow ClO + ClO$	$3.4e-11*\exp(160./T)$

Table 1a. (continued)

	Reaction	Rate Coefficient
(70)	$OClO + O \rightarrow ClO + O_2$	$2.5e-12 * \exp(-950./T)$
(71)	$OClO + NO \rightarrow NO_2 + ClO$	$2.5e-12 * \exp(-600./T)$
(72)	$CH_3CCl_3 + OH \rightarrow 3Cl + \text{products}$	$5.0e-12 * \exp(-1800./T)$
(73)	$Cl_2O_2 + m \rightarrow ClO + ClO$	$3.0e-27 * \exp(8450./T)$ deq $\rightarrow 3.0e-27 * \exp(8450./T)$
(74)	$Cl_2 + OH \rightarrow HOCl + Cl$	$1.4e-12 * \exp(-900./T)$
(75)	$Cl + ClONO_2 \rightarrow Cl_2 + NO_3$	$6.8e-12 * \exp(160./T)$
(76)	$Cl + HO_2 \rightarrow OH + ClO$	$4.1e-11 * \exp(450./T)$
(77)	$Cl + H_2O_2 \rightarrow HCl + HO_2$	$1.1e-11 * \exp(-980./T)$
(78)	$O + HCl \rightarrow OH + Cl$	$1.0e-11 * \exp(-3300./T)$
(79)	$O + ClONO_2 \rightarrow NO_3 + ClO$	$2.9e-12 * \exp(-800./T)$
(80)	$OH + ClONO_2 \rightarrow NO_3 + HOCl$	$1.2e-12 * \exp(-330./T)$
(81)	$BrO + ClO \rightarrow OClO + Br$	$1.6e-12 * \exp(-430./T)$
(82)	$BrO + O \rightarrow Br + O_2$	$3.e-11$
(83)	$OH + HBr \rightarrow H_2O + Br$	$1.1e-11$
(84)	$O(^1D) + HBr \rightarrow OH + Br$	$1.5e-10$
(85)	$OH + BrO \rightarrow HO_2 + Br$	$1.0e-11$
(86)	$Br + O_3 \rightarrow BrO + O_2$	$1.7e-11 * \exp(-800./T)$
(87)	$BrO + NO \rightarrow NO_2 + Br$	$8.8e-12 * \exp(260./T)$
(88)	$BrO + ClO \rightarrow Br + Cl + O_2$	$2.9e-12 * \exp(220./T)$
(89)	$BrO + ClO \rightarrow BrCl + O_2$	$5.8e-13 * \exp(170./T)$
(90)	$BrO + BrO \rightarrow Br + Br + O_2$	$4.0e-12 * \exp(-190./T)$
(91)	$Br + HO_2 \rightarrow HBr + O_2$	$1.5e-11 * \exp(-600./T)$
(92)	$Br + OClO \rightarrow BrO + ClO$	$2.6e-11 * \exp(-1300./T)$
(93)	$BrO + HO_2 \rightarrow HOBr + O_2$	$6.2e-12 * \exp(500./T)$
(94)	$CH_3Br + OH \rightarrow CH_2Br + H_2O$	$4.0e-12 * \exp(-1470./T)$
(95)	$O + HBr \rightarrow OH + Br$	$5.8e-12 * \exp(-1500./T)$

Read $1.2e-10$ as 1.2×10^{-10}; am, air density (number per cubic centimeter). Rate coefficients are expressed in cubic centimeter per second.

Table 1b. Gas Phase Chemical Reactions Included in the Model and Corresponding Reaction Rates [*DeMore et al.*, 1994]

	Reaction	k_x^{300}	n	k_y^{300}	m
(96)	$H + O_2 + m \rightarrow HO_2 + m$	$5.7e-32$	1.6	$7.5e-11$	0.
(97)	$OH + OH + m \rightarrow H_2O_2 + m$	$6.9e-31$	0.8	$1.5e-11$	0.0
(98)	$NO_3 + NO_2 + M \rightarrow N_2O_5$	$2.2e-30$	3.9	$1.5e-12$	0.7
(99)	$NO_2 + OH + m \rightarrow HNO_3 + m$	$2.6e-30$	3.2	$2.4e-11$	1.3
(100)	$NO_2 + HO_2 + m \rightarrow HNO_4 + m$	$1.8e-31$	3.2	$4.7e-12$	1.4
(101)	$O + NO_2 + m \rightarrow NO_3 + m$	$9.0e-32$	2.0	$2.2e-11$	0.0
(102)	$O + NO + m \rightarrow NO_2 + m$	$9.0e-32$	1.5	$3.0e-11$	0.0
(103)	$ClO + NO_2 + m \rightarrow ClONO_2 + m$	$1.8e-31$	3.4	$1.5e-11$	1.9
(104)	$Cl + NO_2 + m \rightarrow ClNO_2 + m$	$1.8e-32$	3.6	$6.e-12$	0.0
(105)	$ClO + ClO + m \rightarrow Cl_2O_2 + m$	$2.2e-32$	3.1	$3.5e-12$	1.0
(106)	$BrO + NO_2 + m \rightarrow BrONO_2 + m$	$5.2e-31$	3.2	$6.9e-12$	2.9

$$k = \frac{k_x M}{1 + \frac{k_x}{k_y}} \times 0.6^{\left[1 + [\log(k_x M/k_y)]^2\right]^{-1}}$$

with $k_x = k_x^{300}\left(\frac{T}{300}\right)^{-n}$ expressed in $cm^3\ s^{-1}$

and $k_y = k_y^{300}\left(\frac{T}{300}\right)^{-m}$ expressed in $cm^3\ s^{-1}$

Table 1c. Photolyses Included in the Model

	Reaction
(107)	$O_2 + h\nu \rightarrow O + O$
(108)	$O_3 + h\nu \rightarrow O + O_2$
(109)	$O_3 + h\nu \rightarrow O(^1D) + O_2$
(110)	$H_2O + h\nu \rightarrow OH + H$
(111)	$H_2O_2 + h\nu \rightarrow 2OH$
(112)	$N_2O + h\nu \rightarrow N_2 + O(^1D)$
(113)	$CH_4 + h\nu \rightarrow CH_3 + H$
(114)	$NO_2 + h\nu \rightarrow NO + O$
(115)	$HNO_3 + h\nu \rightarrow OH + NO_2$
(116)	$HOCl + h\nu \rightarrow Cl + OH$
(117)	$HNO_4 + h\nu \rightarrow NO_2 + HO_2$
(118)	$ClONO_2 + h\nu \rightarrow ClO + NO_2$
(119)	$N_2O_5 + h\nu \rightarrow NO_2 + NO_3$
(120)	$OClO + h\nu \rightarrow O + ClO$
(121)	$Cl_2O_2 + h\nu \rightarrow Cl + ClOO$
(122)	$HCl + h\nu \rightarrow H + Cl$
(123)	$NO + h\nu \rightarrow O + N$
(124)	$CO_2 + h\nu \rightarrow CO + O$
(125)	$CH_3Cl + h\nu \rightarrow Cl + prod.$
(126)	$CH_3CCl_3 + h\nu \rightarrow 3Cl + prod.$
(127)	$CCl_4 + h\nu \rightarrow 4Cl + C$
(128)	$CFCl_3 + h\nu \rightarrow 3Cl + prod.$
(129)	$CF_2Cl_2 + h\nu \rightarrow 2Cl + prod.$
(130)	$NO_3 + h\nu \rightarrow NO_2 + O$
(131)	$Cl_2 + h\nu \rightarrow 2Cl$
(132)	$ClNO_2 + h\nu \rightarrow Cl + NO_2$
(133)	$BrONO_2 + h\nu \rightarrow BrO + NO_2$
(134)	$BrCl + h\nu \rightarrow Br + Cl$
(135)	$HOBr + h\nu \rightarrow Br + OH$
(136)	$CH_3Br + h\nu \rightarrow Br + prod.$
(137)	$HNO_2 + h\nu \rightarrow NO + OH$

Table 2a. Heterogeneous Reactions on the Surface of PSCs

	Reaction	Accommodation Coefficient	Reference
	Type I PSCs		
(1)	$ClONO_2 + H_2O(s) \rightarrow HOCl + HNO_3$	0.02	*Moore et al.* [1990]
(2)	$ClONO_2 + HCl(s) \rightarrow Cl_2 + HNO_3$	0.3	*Hanson and Ravishankara* [1991]
(3)	$N_2O_5 + H_2O(s) \rightarrow 2HNO_3$	0.0006	*Hanson and Ravishankara* [1991]
(4)	$N_2O_5 + HCl(s) \rightarrow ClNO_2 + HNO_3$	0.003	*Hanson and Ravishankara* [1991]
(5)	$HOCl + HCl(s) \rightarrow Cl_2 + H_2O$	0.1	*DeMore et al.* [1994]
	Type II PSCs		
(6)	$ClONO_2 + H_2O(s) \rightarrow HOCl + HNO_3$	0.3	*Hanson and Ravishankara* [1991]
(7)	$ClONO_2 + HCl(s) \rightarrow Cl_2 + HNO_3$	0.2	*DeMore et al.* [1994]
(8)	$N_2O_5 + H_2O(s) \rightarrow 2HNO_3$	0.03	*Quinlan et al.* [1990]
(9)	$N_2O_5 + HCl(s) \rightarrow ClNO_2 + HNO_3$	0.03	*DeMore et al.* [1994]
(10)	$HOCl + HCl(s) \rightarrow Cl_2 + H_2O$	0.3	*DeMore et al.* [1994]

PSC, polar stratospheric cloud.

Table 2b. Heterogeneous Reactions on the Surface of Sulfate Aerosols

	Reaction	Accommodation Coefficient	Reference
(11)	$ClONO_2 + H_2O(s) \rightarrow HOCl + HNO_3$	see *Hanson et al.* [1994]	*Hanson et al.* [1994]
(12)	$ClONO_2 + HCl(s) \rightarrow Cl_2 + HNO_3$	see *Hanson et al.* [1994]	*Hanson et al.* [1994]
(13)	$N_2O_5 + H_2O(s) \rightarrow 2HNO_3$	0.1	*DeMore et al.* [1994]
(14)	$HOCl + HCl(s) \rightarrow Cl_2 + H_2O$	see *Hanson et al.* [1994]	*Hanson et al.* [1994]
(15)	$BrONO_2 + H_2O(s) \rightarrow Cl_2 + HNO_3$	0.4	*Danilin and McConell* [1994]
(16)	$HOBr + HCl(s) \rightarrow BrCl + H_2O$	0.2 (60% weight of sulfate)	see *Hanson and Ravishankara* [1995]

Table 3. Chemical reactions considered in MOZART

No.	Reaction	Rate	Ref.
1	$O(^1D) + N_2 \rightarrow O + N_2$	$k_1 = 1.80E\text{-}11\ \exp(110/T)$	[1]
2	$O(^1D) + O_2 \rightarrow O + O_2$	$k_2 = 3.20E\text{-}11\ \exp(70/T)$	[1]
3	$O(^1D) + H_2O \rightarrow 2\ OH$	$k_3 = 2.20E\text{-}10$	[1]
4	$O + O_2 + M \rightarrow O_3 + M$	$k_4 = 6.00E\text{-}34\ [M]\ (300/T)^{2.3}$	[1]
5	$O + O_3 \rightarrow 2\ O_2$	$k_5 = 8.00E\text{-}12\ \exp(-2060/T)$	[1]
6	$O + OH \rightarrow HO_2 + O_2$	$k_6 = 2.20E\text{-}11\ \exp(120/T)$	[1]
7	$O + HO_2 \rightarrow OH + O_2$	$k_7 = 3.00E\text{-}11\ \exp(200/T)$	[1]
8	$OH + O_3 \rightarrow HO_2 + O_2$	$k_8 = 1.60E\text{-}12\ \exp(-940/T)$	[1]
9	$HO_2 + O_3 \rightarrow OH + 2\ O_2$	$k_9 = 1.10E\text{-}14\ \exp(-500/T)$	[1]
10	$HO_2 + HO_2 \rightarrow H_2O_2$	$k_{10} = (k_a + k_b)\ k_c$ $k_a = 2.30E\text{-}13\ \exp(600/T)$ $k_b = 1.70E\text{-}33\ [M]\ \exp(1000/T)$ $k_c = 1 + 1.40E\text{-}21\ [H_2O]\ \exp(2200/T)$	[1]
11	$H_2O_2 + OH \rightarrow H_2O + HO_2$	$k_{11} = 2.90E\text{-}12\ \exp(-160/T)$	[1]
12	$OH + HO_2 \rightarrow H_2O + O_2$	$k_{12} = 4.80E\text{-}11\ \exp(250/T)$	[1]
13	$OH + OH \rightarrow H_2O + O$	$k_{13} = 4.20E\text{-}12\ \exp(-240/T)$	[1]
14	$H_2 + OH \rightarrow H_2O + HO_2$	$k_{14} = 5.50E\text{-}12\ \exp(-2000/T)$	[1]
15	$H_2 + O(^1D) \rightarrow HO_2 + OH$	$k_{15} = 1.00E\text{-}10$	[1]
16	$N_2O + O(^1D) \rightarrow 2\ NO$	$k_{16} = 6.70E\text{-}11$	[1]
17	$N_2O + O(^1D) \rightarrow N_2 + O_2$	$k_{17} = 4.90E\text{-}11$	[1]
18	$N + O_2 \rightarrow NO + O$	$k_{18} = 1.50E\text{-}11\ \exp(-3600/T)$	[1]
19	$N + NO \rightarrow N_2 + O$	$k_{19} = 2.10E\text{-}11\ \exp(100/T)$	[1]
20	$NO + HO_2 \rightarrow NO_2 + OH$	$k_{20} = 3.50E\text{-}12\ \exp(250/T)$	[1]
21	$NO + O_3 \rightarrow NO_2 + O_2$	$k_{21} = 2.00E\text{-}12\ \exp(-1400/T)$	[1]
22	$NO_2 + O \rightarrow NO + O_2$	$k_{22} = 6.50E\text{-}12\ \exp(120/T)$	[1]
23	$NO_2 + O_3 \rightarrow NO_3 + O_2$	$k_{23} = 1.20E\text{-}13\ \exp(-2450/T)$	[1]
24	$NO_3 + HO_2 \rightarrow 0.4\ HNO_3 + 0.6\ OH + 0.6\ NO_2$	$k_{24} = 2.30E\text{-}12\ \exp(170/T)$	[2]
25	$NO_2 + NO_3 + M \rightarrow N_2O_5 + M$	$k_0 = 2.20E\text{-}30\ (300/T)^{3.9}$ $k_\infty = 1.50E\text{-}12\ (300/T)^{0.7}$ $F_c = 0.6$	[1]
26	$N_2O_5 + M \rightarrow NO_2 + NO_3 + M$	$k_{26} = k_{25}\ 3.7E26\ \exp(-11000/T)$	[1]
27	$N_2O_5 + H_2O \rightarrow 2\ HNO_3$	$k_{27} = 2.00E\text{-}21$	[1]
28	$NO_2 + OH + M \rightarrow HNO_3 + M$	$k_0 = 2.50E\text{-}30\ (300/T)^{4.4}$ $k_\infty = 1.60E\text{-}11\ (300/T)^{1.7}$ $F_c = 0.6$	[1]
29	$HNO_3 + OH \rightarrow NO_3 + H_2O$	$k_{29} = k_a + 7.20E\text{-}15\ \exp(785/T)$ $k_a = k_b\ /\ (1 + k_b\ /\ k_c)$ $k_b = 1.90E\text{-}33\ \exp(725/T)\ [M]$ $k_c = 4.10E\text{-}16\ \exp(1440/T)$	[1]
30	$NO_3 + NO \rightarrow 2\ NO_2$	$k_{30} = 1.50E\text{-}11\ \exp(170/T)$	[1]
31	$NO_2 + HO_2 + M \rightarrow HO_2NO_2 + M$	$k_0 = 1.80E\text{-}31\ (300/T)^{3.2}$ $k_\infty = 4.70E\text{-}12\ (300/T)^{1.4}$ $F_c = 0.6$	[1]
32	$HO_2NO_2 + M \rightarrow HO_2 + NO_2 + M$	$k_{32} = k_{31}\ 4.7E26\ \exp(-10900/T)$	[1]
33	$HO_2NO_2 + OH \rightarrow H_2O + NO_2 + O_2$	$k_{33} = 1.30E\text{-}12\ \exp(380/T)$	[1]
34	$CH_4 + OH \rightarrow CH_3O_2 + H_2O$	$k_{34} = 2.45E\text{-}12\ \exp(-1775/T)$	[1]
35	$CH_4 + O(^1D) \rightarrow CH_3O_2 + OH$	$k_{35} = 1.40E\text{-}10$	[1]
36	$CH_4 + O(^1D) \rightarrow H_2 + CH_2O$	$k_{36} = 1.40E\text{-}11$	[1]
37	$CH_3O_2 + NO \rightarrow CH_2O + NO_2 + HO_2$	$k_{37} = 3.00E\text{-}12\ \exp(280/T)$	[1]
38	$CH_3O_2 + CH_3O_2 \rightarrow 1.4\ CH_2O + 0.8\ HO_2$	$k_{38} = 2.50E\text{-}13\ \exp(190/T)$	[1]
39	$CH_3O_2 + HO_2 \rightarrow CH_3OOH + O_2$	$k_{39} = 3.80E\text{-}13\ \exp(800/T)$	[1]
40	$CH_3OOH + OH \rightarrow 0.58\ CH_3O_2 + 0.42\ OH + 0.42\ CH_2O$	$k_{40} = 3.80E\text{-}12\ \exp(200/T)$	[1]
41	$CH_2O + OH \rightarrow CO + H_2O + HO_2$	$k_{41} = 1.10E\text{-}11$	[1]
42	$CH_2O + NO_3 \rightarrow CO + HO_2 + HNO_3$	$k_{42} = 6.00E\text{-}13\ \exp(-2058/T)$	[3]
43	$CO + OH \rightarrow CO_2 + HO_2$	$k_{43} = 1.50E\text{-}13\ (1 + 0.6\ P)$	[1]
44	$C_2H_6 + OH \rightarrow C_2H_5O_2 + H_2O$	$k_{44} = 8.70E\text{-}12\ \exp(-1070/T)$	[1]
45	$C_2H_5O_2 + NO \rightarrow CH_3CHO + HO_2 + NO_2$	$k_{45} = 2.60E\text{-}12\ \exp(365/T)$	[1]

Table 3. (continued)

No.	Reaction	Rate	Ref.
46	$C_2H_5O_2 + HO_2 \rightarrow C_2H_5OOH + O_2$	$k_{46} = 7.50E\text{-}13\ \exp(700/T)$	[1]
47	$C_2H_5O_2 + CH_3O_2 \rightarrow 0.7\ CH_2O + 0.3\ CH_3CHO + HO_2$	$k_{47} = 3.75E\text{-}13\ \exp(-40/T)$	[4]
48	$C_2H_5O_2 + C_2H_5O_2 \rightarrow 1.6\ CH_3CHO + 1.2\ HO_2$	$k_{48} = 6.50E\text{-}14$	[1]
49	$C_2H_5OOH + OH \rightarrow 0.5\ C_2H_5O_2 + 0.5\ CH_3CHO + 0.5\ OH$	$k_{49} = 3.80E\text{-}12\ \exp(200/T)$	[4]
50	$C_3H_8 + OH \rightarrow C_3H_7O_2 + H_2O$	$k_{50} = 1.00E\text{-}11\ \exp(-660/T)$	[1]
51	$C_3H_7O_2 + NO \rightarrow 0.82\ CH_3COCH_3 + NO_2 + HO_2$	$k_{51} = 4.20E\text{-}12\ \exp(180/T)$	[5]
52	$C_3H_7O_2 + HO_2 \rightarrow C_3H_7OOH + O_2$	$k_{52} = 7.50E\text{-}13\ \exp(700/T)$	[6]
53	$C_3H_7O_2 + CH_3O_2 \rightarrow 0.5\ CH_2O + HO_2 + 0.82\ CH_3COCH_3$	$k_{53} = 3.75E\text{-}13\ \exp(-40/T)$	[6]
54	$C_3H_7OOH + OH \rightarrow H_2O + C_3H_7O_2$	$k_{54} = 3.80E\text{-}12\ \exp(200/T)$	[6]
55	$CH_3COCH_3 + OH \rightarrow CH_3COCH_2O_2 + H_2O$	$k_{55} = 2.20E\text{-}12\ \exp(-685/T)$	[1]
56	$CH_3COCH_2O_2 + NO \rightarrow CH_3COCH_2O + NO_2$	$k_{56} = 4.20E\text{-}12\ \exp(180/T)$	[6]
57	$CH_3COCH_2O_2 + HO_2 \rightarrow CH_3COCH_2OOH + O_2$	$k_{57} = 7.50E\text{-}13\ \exp(700/T)$	[6]
58	$CH_3COCH_2OOH + OH \rightarrow CH_3COCH_2O_2 + H_2O$	$k_{58} = 3.80E\text{-}12\ \exp(200/T)$	[6]
59	$CH_3COCH_2O + M \rightarrow CH_3CO_3 + CH_2O + M$	$k_{59} = 8.70E\text{+}13\ \exp(-7300/T)$	[6]
60	$CH_3COCH_2O + O_2 \rightarrow CH_3COCHO + HO_2$	$k_{60} = 6.50E\text{-}14\ \exp(-1400/T)$	[6]
61	$C_4H_{10} + OH \rightarrow 0.3\ ISO1$	$k_{61} = 1.55E\text{-}11\ \exp(-540/T)$	[7]
62	$C_3H_6 + OH + M \rightarrow C_3H_6OHO_2 + M$	$k_0 = 8.00E\text{-}27\ (300/T)^{3.5}$ $k_\infty = 3.00E\text{-}11$ $F_c = 0.5$	[5]
63	$C_3H_6 + O_3 \rightarrow 1.065\ CH_2O + 1.17\ HO_2 + 0.855\ OH + 0.16\ CH_4 + 0.74\ CO + CH_3CHO + 0.575\ CH_3O_2$	$k_{63} = 3.25E\text{-}15\ \exp(-1900/T)$	[1]
64	$C_3H_6 + NO_3 \rightarrow ONIT$	$k_{64} = 4.00E\text{-}15$	[4]
65	$C_3H_6OHO_2 + NO \rightarrow CH_3CHO + CH_2O + HO_2 + NO_2$	$k_{65} = 4.20E\text{-}12\ \exp(180/T)$	[4]
66	$C_3H_6OHO_2 + HO_2 \rightarrow C_3H_6OHOOH + O_2$	$k_{66} = 6.50E\text{-}13\ \exp(650/T)$	[4]
67	$C_3H_6OHOOH + OH \rightarrow 0.5\ C_3H_6OHO_2 + 0.5\ OH + H_2O$	$k_{67} = 3.80E\text{-}12\ \exp(200/T)$	[4]
68	$CH_3CHO + OH \rightarrow CH_3CO_3 + H_2O$	$k_{68} = 5.60E\text{-}12\ \exp(270/T)$	[1]
69	$CH_3CHO + NO_3 \rightarrow CH_3CO_3 + HNO_3$	$k_{69} = 1.40E\text{-}12\ \exp(-1900/T)$	[1]
70	$CH_3CO_3 + NO \rightarrow CH_3O_2 + CO_2 + NO_2$	$k_{70} = 5.30E\text{-}12\ \exp(260/T)$	[1]
71	$CH_3CO_3 + NO_2 + M \rightarrow PAN + M$	$k_0 = 9.70E\text{-}29\ (300/T)^{5.6}$ $k_\infty = 9.30E\text{-}12\ (300/T)^{1.5}$ $F_c = 0.6$	[1]
72	$PAN + M \rightarrow CH_3CO_3 + NO_2 + M$	$k_{72} = k_{71}\ 1.11E28\ \exp(-14000/T)$	[1]
73	$CH_3CO_3 + HO_2 \rightarrow 0.67\ CH_3COOOH + 0.33\ CH_3COOH + 0.33\ O_3$	$k_{73} = 4.30E\text{-}13\ \exp(1040/T)$	[1]
74	$CH_3CO_3 + CH_3O_2 \rightarrow CH_3O_2 + CH_2O + HO_2 + CO_2$	$k_{74} = 1.80E\text{-}09\ \exp(-1800/T)$	[8]
75	$CH_3CO_3 + CH_3O_2 \rightarrow CH_2O + CH_3COOH + O_2$	$k_{75} = 4.10E\text{-}15\ \exp(2100/T)$	[8]
76	$CH_3CO_3 + CH_3CO_3 \rightarrow 2\ CH_3O_2 + 2\ CO_2$	$k_{76} = 2.90E\text{-}12\ \exp(500/T)$	[1]
77	$CH_3COOOH + OH \rightarrow CH_3CO_3 + H_2O$	$k_{77} = 1.00E\text{-}11$	[4]
78	$C_2H_4 + OH + M \rightarrow 0.6667\ C_3H_6OHO_2 + M$	$k_0 = 1.00E\text{-}28\ (300/T)^{0.8}$ $k_\infty = 8.80E\text{-}12$ $F_c = 0.6$	[1]
79	$C_2H_4 + O_3 \rightarrow CH_2O + 0.52\ HO_2 + 0.42\ CO$	$k_{79} = 1.20E\text{-}14\ \exp(-2630/T)$	[1]
80	$ISO + OH \rightarrow ISO1$	$k_{80} = 2.50E\text{-}11\ \exp(-450/T)$	[4]
81	$ISO + O_3 \rightarrow 1.32\ MACR + 0.52\ MVK + 0.9\ O + 1.565\ CH_2O + 0.12\ HO_2 + 1.36\ OH + 0.14\ C_3H_6 + 0.38\ CO$	$k_{81} = 1.20E\text{-}14\ \exp(-2013/T)$	[9]
82	$ISO + NO_3 \rightarrow ONIT$	$k_{82} = 3.03E\text{-}12\ \exp(-446/T)$	[9]
83	$ISO1 + NO \rightarrow 0.84\ MVK + 1.16\ MACR + 2\ CH_2O + 2\ HO_2 + 2\ NO_2$	$k_{83} = 3.70E\text{-}13\ \exp(180/T)$	[4]
84	$ISO1 + NO \rightarrow 1.18\ CH_3CO_3 + 2\ CH_2O + 1.18\ CH_2OHCHO + 1.18\ NO_2 + 0.82\ ONIT$	$k_{84} = 5.00E\text{-}13\ \exp(180/T)$	[4]
85	$ISO1 + HO_2 \rightarrow 0.126\ MVK + 0.174\ MACR + 0.3\ CH_2O + 0.3\ HO_2$	$k_{85} = 7.50E\text{-}13\ \exp(750/T)$	[9]
86	$ISO1 + CH_3O_2 \rightarrow MACR + 2\ CH_2O + 2\ HO_2$	$k_{86} = 1.30E\text{-}14$	[4]
87	$ISO1 + CH_3CO_3 \rightarrow MACR + HO_2 + CH_2O$	$k_{87} = 4.90E\text{-}14$	[4]
88	$MVK + OH \rightarrow MOHO_2$	$k_{88} = 4.13E\text{-}12\ \exp(452/T)$	[9]
89	$MVK + O_3 \rightarrow 0.1\ CO + 0.12\ HO_2 + 0.08\ CH_3CHO + 1.64\ CH_3COCHO + 1.6\ CH_2O + + 0.4\ O + .16\ OH$	$k_{89} = 4.00E\text{-}15\ \exp(-2000/T)$	[9]
90	$MACR + OH \rightarrow 0.5\ MOHO_2 + 0.5\ MCO_3$	$k_{90} = 1.86E\text{-}11\ \exp(175/T)$	[9]

Table 3. (continued)

No.	Reaction	Rate	Ref.
91	$MACR + O_3 \rightarrow 0.55\ HO_2 + 0.43\ OH + 1.6\ CH_3COCHO + 1.4\ CH_2O + 0.4\ O + 0.4\ CO$	$k_{91} = 4.40E\text{-}15\ \exp(-2500/T)$	[9]
92	$MOHO_2 + NO \rightarrow CH_2OHCHO + CH_3CO_3 + NO_2$	$k_{92} = 3.50E\text{-}12\ \exp(180/T)$	[4]
93	$MOHO_2 + NO \rightarrow ONIT$	$k_{93} = 4.50E\text{-}13\ \exp(180/T)$	[4]
94	$MOHO_2 + HO_2 \rightarrow 0.3\ CH_3CO_3 + 0.3\ CH_2OHCHO$	$k_{94} = 7.50E\text{-}13\ \exp(700/T)$	[4]
95	$CH_2OHCHO + OH \rightarrow 0.5\ CH_3CO_3 + 0.5\ HO_2$	$k_{95} = 6.00E\text{-}12\ \exp(250/T)$	[4]
96	$CH_2OHCHO + NO_3 \rightarrow CH_3CO_3 + HNO_3$	$k_{96} = 1.40E\text{-}12\ \exp(-1900/T)$	[4]
97	$MCO_3 + NO \rightarrow CH_3COCH_2O + NO_2$	$k_{97} = 2.40E\text{-}11$	[1]
98	$MCO_3 + NO_2 \rightarrow MPAN$	$k_0 = 9.70E\text{-}29\ (300/T)^{5.6}$ $k_\infty = 9.30E\text{-}12\ (300/T)^{1.5}$ $F_c = 0.6$	[1]
99	$MPAN + M \rightarrow MCO_3 + NO_2 + M$	$k_{99} = k_{86}\ 1.11E28\ \exp(-14000/T)$	[1]
100	$MCO_3 + HO_2 \rightarrow MOHO_2$	$k_{100} = 4.50E\text{-}13\ \exp(1040/T)$	[4]
101	$MCO_3 + CH_3O_2 \rightarrow CH_2O + HO_2 + CH_3COCH_2O$	$k_{101} = 2.20E\text{-}12\ \exp(490/T)$	[8]
102	$MCO_3 + CH_3CO_3 \rightarrow CH_3COCH_2O + CH_3O_2$	$k_{102} = 5.00E\text{-}12\ \exp(550/T)$	[4]
103	$MCO_3 + MCO_3 \rightarrow 2\ CH_3COCH_2O$	$k_{103} = 2.50E\text{-}12\ \exp(550/T)$	[4]
104	$ONIT + OH \rightarrow NO_2 + MOHO_2$	$k_{104} = 6.80E\text{-}13$	[4]
105	$C_{10}H_{16} + OH \rightarrow 1.64\ ISO1 + CH_3COCH_3$	$k_{105} = 1.20E\text{-}11\ \exp(444/T)$	[10]
106	$C_{10}H_{16} + O_3 \rightarrow 2.244\ MACR + 0.884\ MVK + 1.53\ O + 2.312\ OH + 0.238\ C_3H_6 + 2.652\ CH_2O + 0.646\ CO + 0.204\ HO_2$	$k_{106} = 9.90E\text{-}16\ \exp(-730/T)$	[4]
107	$C_{10}H_{16} + NO_3 \rightarrow 1.7\ ISO1 + NO_2$	$k_{107} = 5.60E\text{-}11\ \exp(-650/T)$	[4]
108	$N_2O_5 + SO_4^= \rightarrow HNO_3 + HNO_3$	$k_{108} = f([SO_4^=], T, [H_2O])$	[4]
109	$NO_3 + SO_4^= \rightarrow HNO_3$	$k_{109} = f([SO_4^=], T, [H_2O])$	[4]
110	$MVK + SO_4^= \rightarrow$ Products	$k_{110} = f([SO_4^=], T, [H_2O])$	[4]
111	$MACR + SO_4^= \rightarrow$ Products	$k_{111} = f([SO_4^=], T, [H_2O])$	[4]
112	$CH_3COCHO + SO_4^= \rightarrow$ Products	$k_{112} = f([SO_4^=], T, [H_2O])$	[4]

T is temperature (K), [M] atmospheric density (cm^{-3}), [H_2O] water vapor density (cm^{-3}), P pressure (hPa), [$SO_4^=$] sulfate density. References: 1, *DeMore et al.* [1997]; 2, *Hall et al.* [1988]; 3, *Cantrell et al.* [1985]; 4, *Müller and Brasseur* [1995]; 5, *Atkinson et al.* [1996]; 6, *Kanakidou et al.* [1991]; 7, *Atkinson* [1985]; 8, *Moorgat et al.* [1989]; 9, *Zimmermann and Poppe* [1996]; 10, *Carter* [1990]. The three-body reaction rates are calculated from:

$$k = \frac{k_0[M]}{1 + k_0[M]/k_\infty} F_c^{\left\{1+[\lg(k_0[M]/k_\infty)]^2\right\}^{-1}}$$

Table 4. Photolytic reactions considered in MOZART

No.	Reaction	Ref.
1	$O_2 + h\nu \rightarrow O + O$	[1]
2	$O_3 + h\nu \rightarrow O(^1D) + O_2$	[1]
3	$O_3 + h\nu \rightarrow O + O_2$	[1]
4	$N_2O + h\nu \rightarrow O(^1D) + N_2$	[1]
5	$NO + h\nu \rightarrow N + O$	[1]
6	$NO_2 + h\nu \rightarrow NO + O$	[1]
7	$N_2O_5 + h\nu \rightarrow NO_2 + NO_3$	[1]
8	$HNO_3 + h\nu \rightarrow NO_2 + OH$	[1]
9	$NO_3 + h\nu \rightarrow 0.89\ NO_2 + 0.11\ NO + 0.89\ O_3$	[2]
10	$HO_2NO_2 + h\nu \rightarrow NO_2 + HO_2$	[1]
11	$CH_3OOH + h\nu \rightarrow CH_2O + HO_2 + OH$	[1]
12	$CH_2O + h\nu \rightarrow CO + 2\ HO_2$	[1]
13	$CH_2O + h\nu \rightarrow CO + H_2$	[1]
14	$H_2O + h\nu \rightarrow OH + HO_2$	[1]
15	$H_2O_2 + h\nu \rightarrow OH + OH$	[1]
16	$CH_3CHO + h\nu \rightarrow CH_3O_2 + CO + HO_2$	[2]
17	$C_3H_6OHOOH + h\nu \rightarrow CH_3CHO + CH_2O + HO_2 + OH$	[3]
18	$CH_3COOOH + h\nu \rightarrow CH_3O_2 + OH$	[3]
19	$PAN + h\nu \rightarrow CH_3CO_3 + NO_2$	[1]
20	$MPAN + h\nu \rightarrow MCO_3 + NO_2$	[3]
21	$CH_2OHCHO + h\nu \rightarrow CH_2O + CO + 2\ HO_2$	[3]
22	$MACR + h\nu \rightarrow MCO_3 + CO + 0.6\ CH_3COCHO + 0.4\ CH_3CO_3 + 0.4\ CH_2O + 2.6\ HO_2$	[3]
23	$MVK + h\nu \rightarrow CH_3CO_3 + HO_2 + 0.25\ CH_2O + 0.25\ CO$	[3]
24	$C_2H_5OOH + h\nu \rightarrow CH_3CHO + HO_2 + OH$	[3]
25	$C_3H_7OOH + h\nu \rightarrow 0.82\ CH_3COCH_3 + OH + HO_2$	[4]
26	$CH_3COCH_2OOH + h\nu \rightarrow CH_3COCH_2O + OH$	[4]
27	$CH_3COCH_3 + h\nu \rightarrow CH_3CO_3 + CH_3O_2$	[5]
28	$CH_3COCHO + h\nu \rightarrow CH_3CO_3 + CO + HO_2$	[2]

References: 1, *DeMore et al.* [1997]; 2, *Madronich and Calvert* [1989]; 3, *Müller and Brasseur* [1995]; 4, *Kanakidou et al.* [1991]; 5, *Gierczak et al.* [1998].

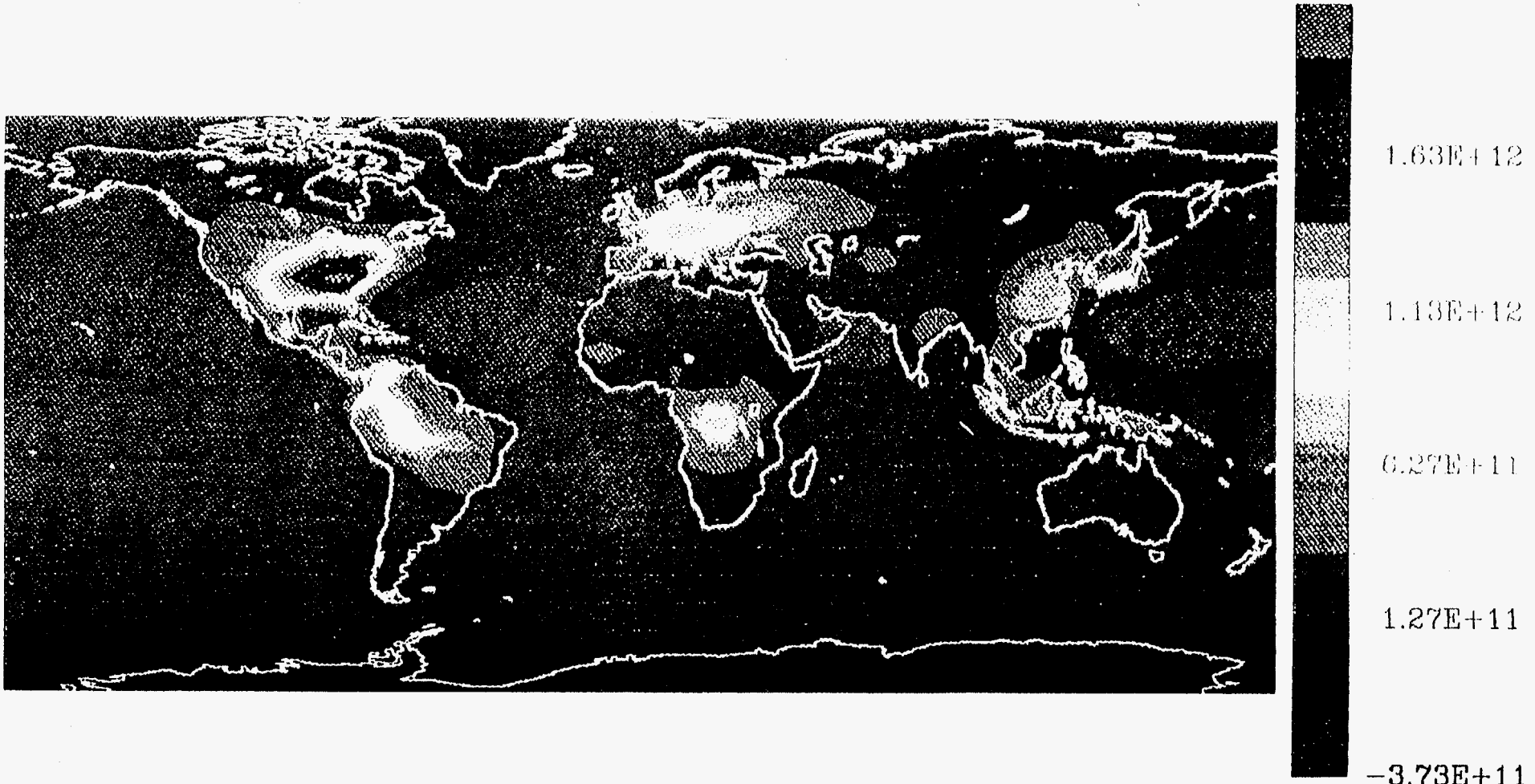

Figure 1. Vertically integrated net photochemical chemical production of ozone (#/cm^2/s) in the troposphere provided by the IMAGES model for July.

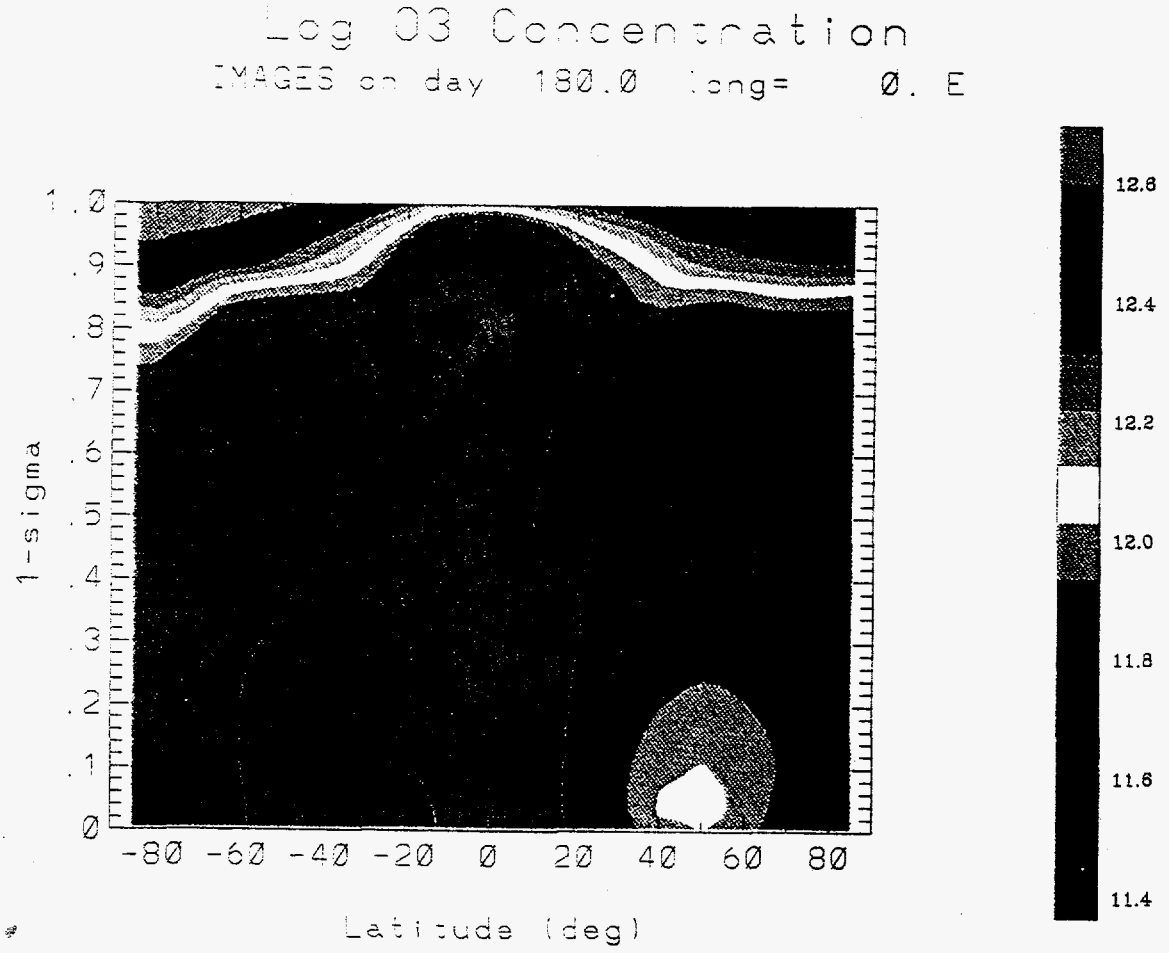

Figure 2. Meridional cross-section of the ozone number density (logarithmic scale of #/cm^3) on the Greenwich meridian. Note that the vertical scale is expressed as a function of the sigma coordinates.

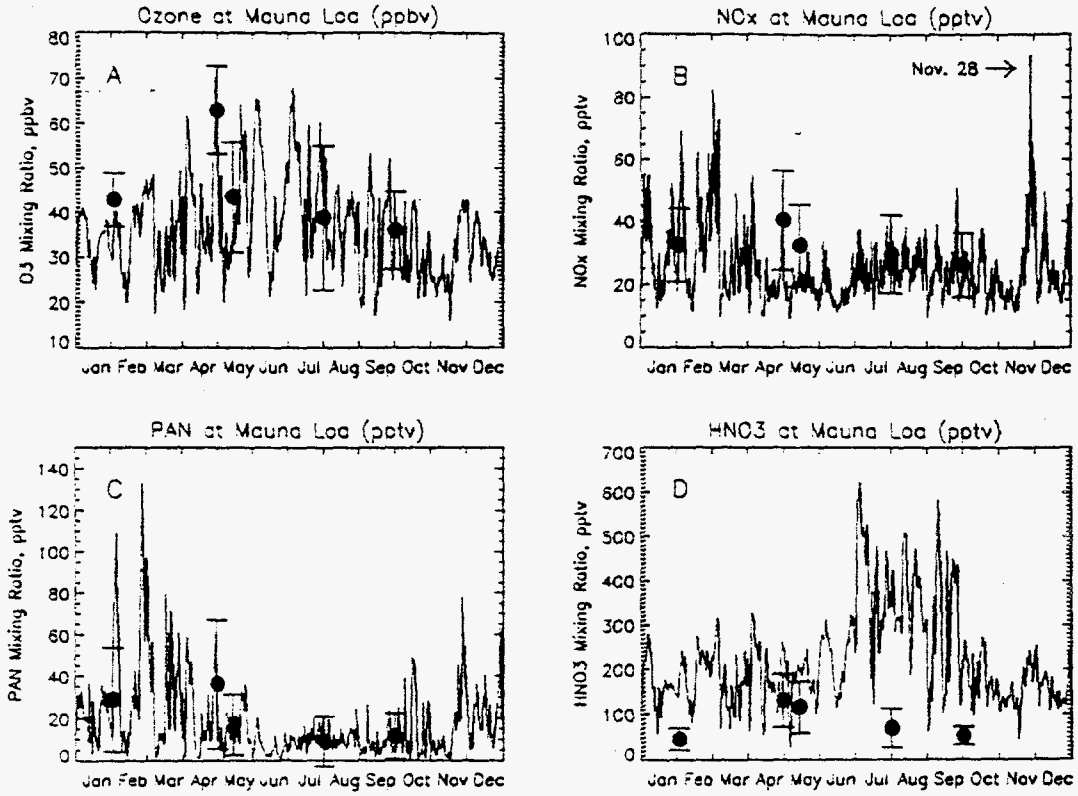

Figure 3. Seasonal variation of (a) ozone (ppbv), (b) NO_x (pptv), (c) PAN (pptv), (d) HNO_3 (pptv) calculated by the CTM (solid line) and compared to the mean values and standard deviations during the MLOPEX 1 and 2 intensives. Note that seasonal variation goes from January 1 to December 31 and that observed values, averaged over each intensive duration, refer respectively to MLOPEX 2b (February 1), 2c (May 1), 1 (May 15), 2d (August 1) and 2a (October 1). For NO_x, the arrow indicates the NO_x event occuring on November 28

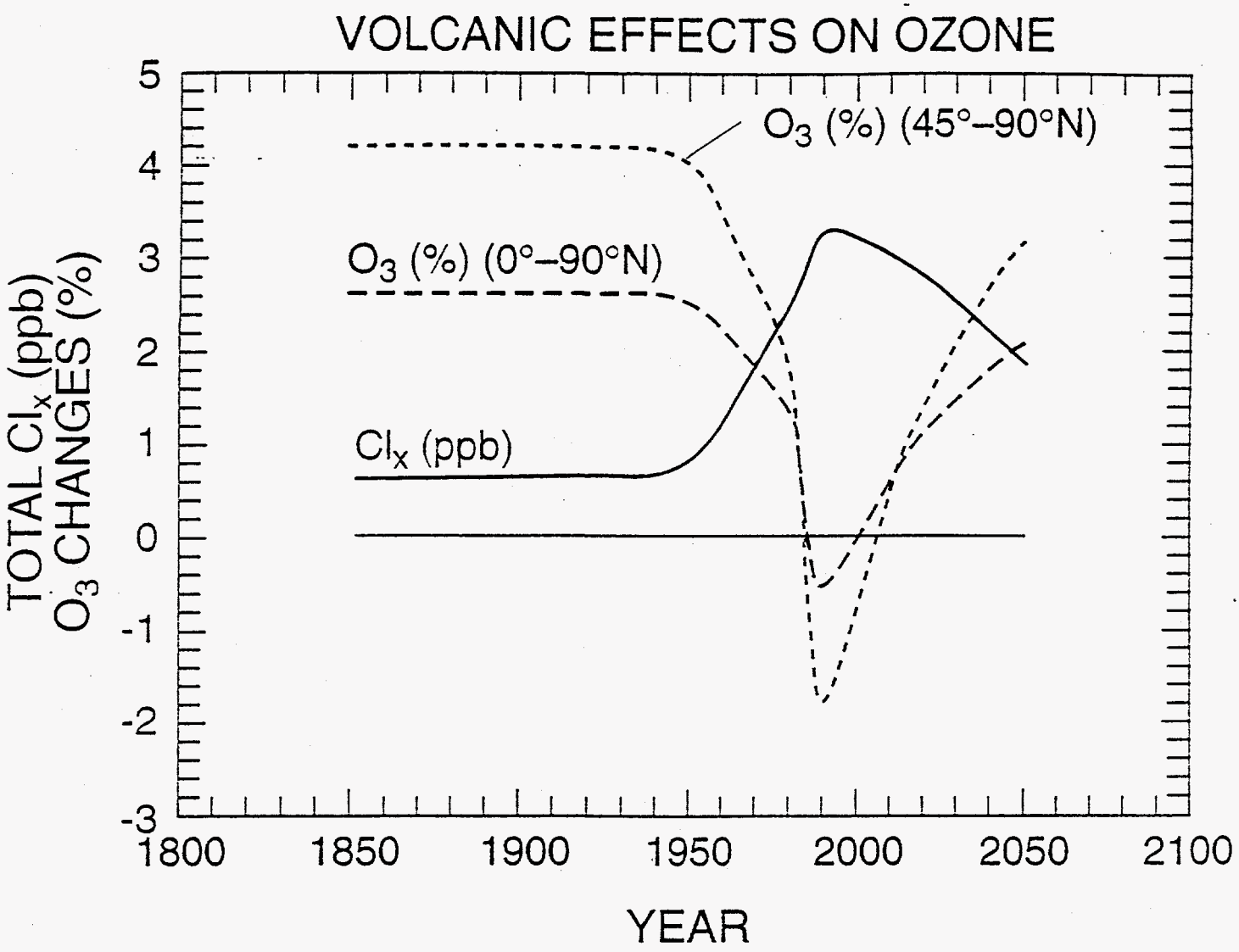

Figure 4. Effect of a Mt. Pinatubo-like volcanic eruption on total ozone (percent) calculated as a function of time (year) of the potential eruption between year 1850 and year 2050 (averaged column in the northern hemisphere and north of 45°N, respectively). The corresponding chlorine loading is also represented.

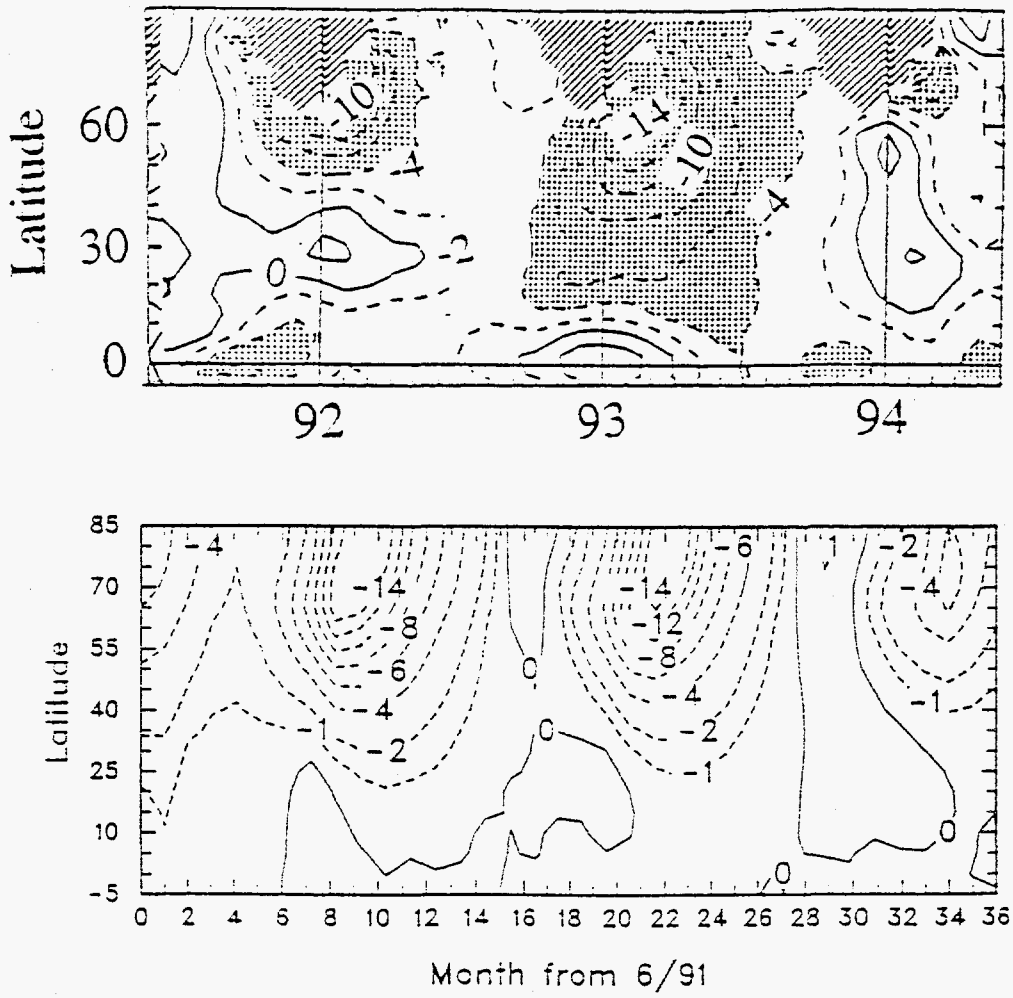

Figure 5. (top) Total ozone anomaly (percent) observed from total ozone mapping spectrometer (TOMS) [*Randel et al.*, 1995], and (bottom) calculated total ozone changes (percent) due to heterogeneous reactions occurring at the surface of enhanced sulfate aerosols following the eruption of Mount Pinatubo in the northern hemisphere. Reaction probabilities are calculated using the 1991-1994 mean temperature (case A).

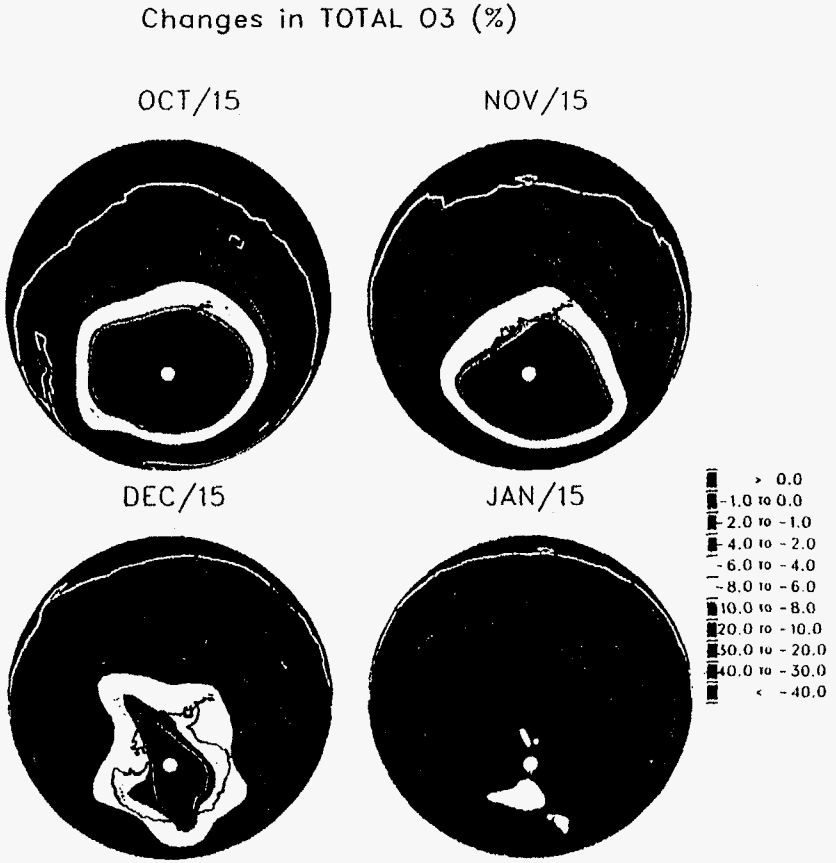

Figure 6. Calculated changes in total column ozone (%) in the southern hemisphere between October and January due to the effects of PSCs.

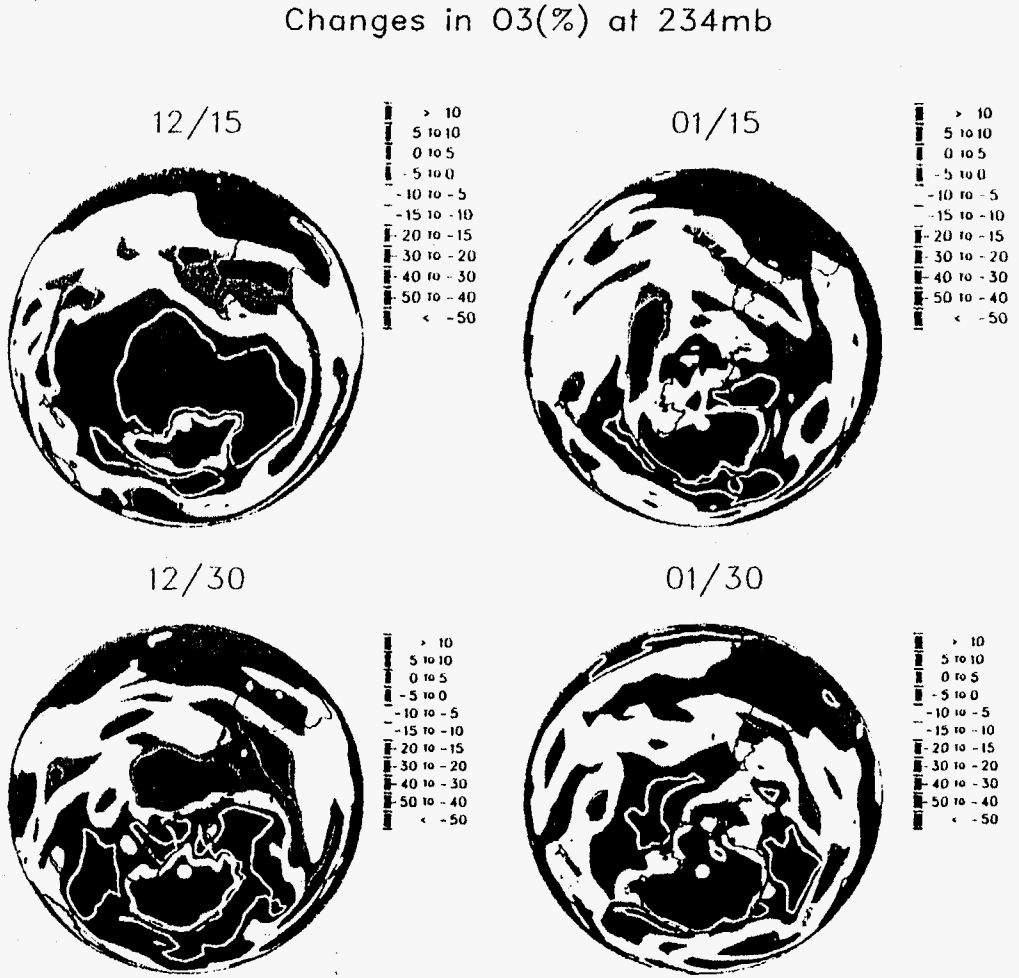

Figure 7. Relative changes in the ozone concentration (%) calculated in the upper troposphere (234 mbar) and the southern hemisphere between December and January caused by the effects of PSCs.

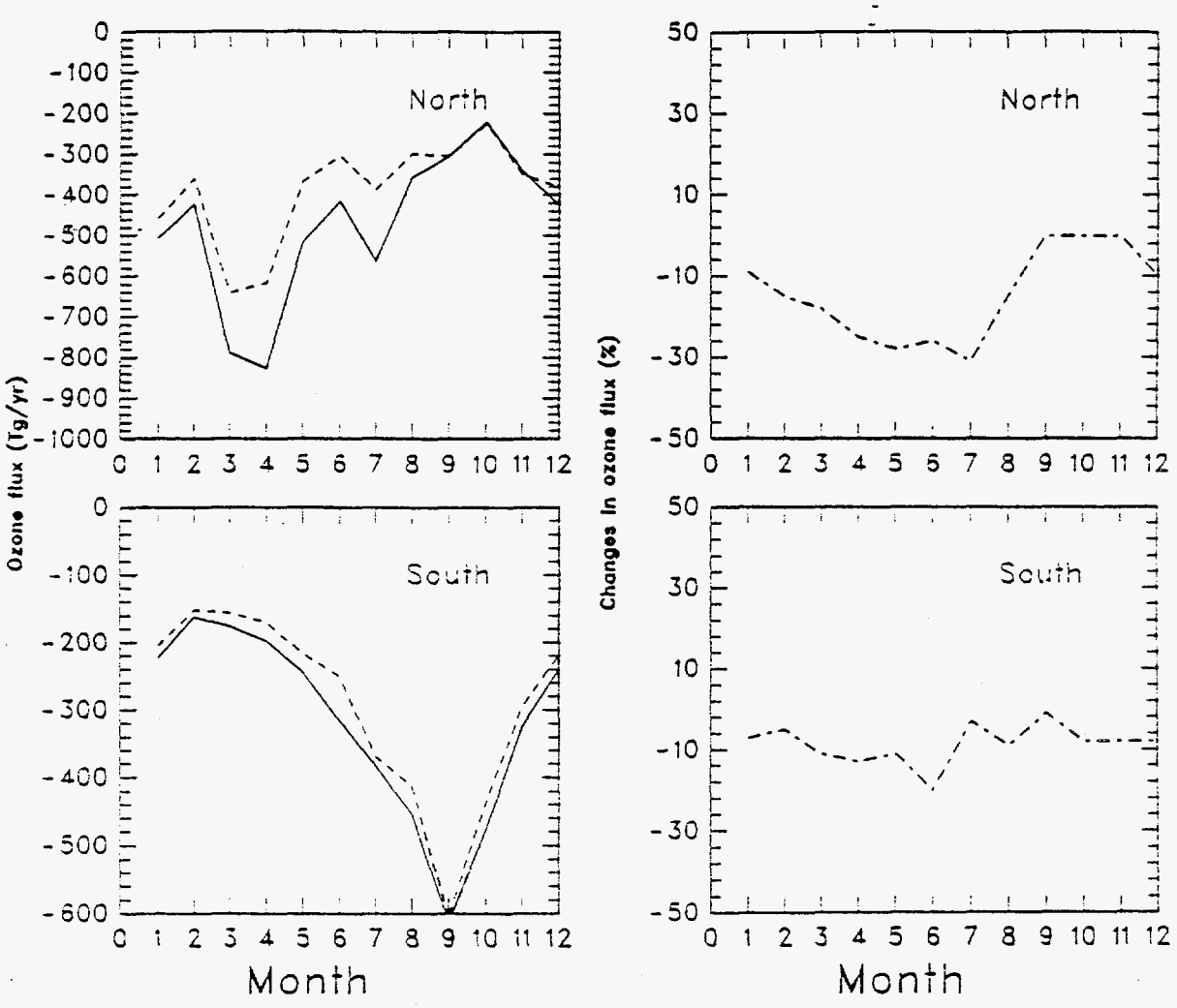

Figure 8. Calculated effect of volcanic aerosols on the ozone mass flux cross the tropopause. (left) The solid line represents the calculation with background aerosols and the dash line gives the calculation with volcanic aerosols. (right) The difference (%) in the ozone mass flux cross the tropopause between the two calculations.

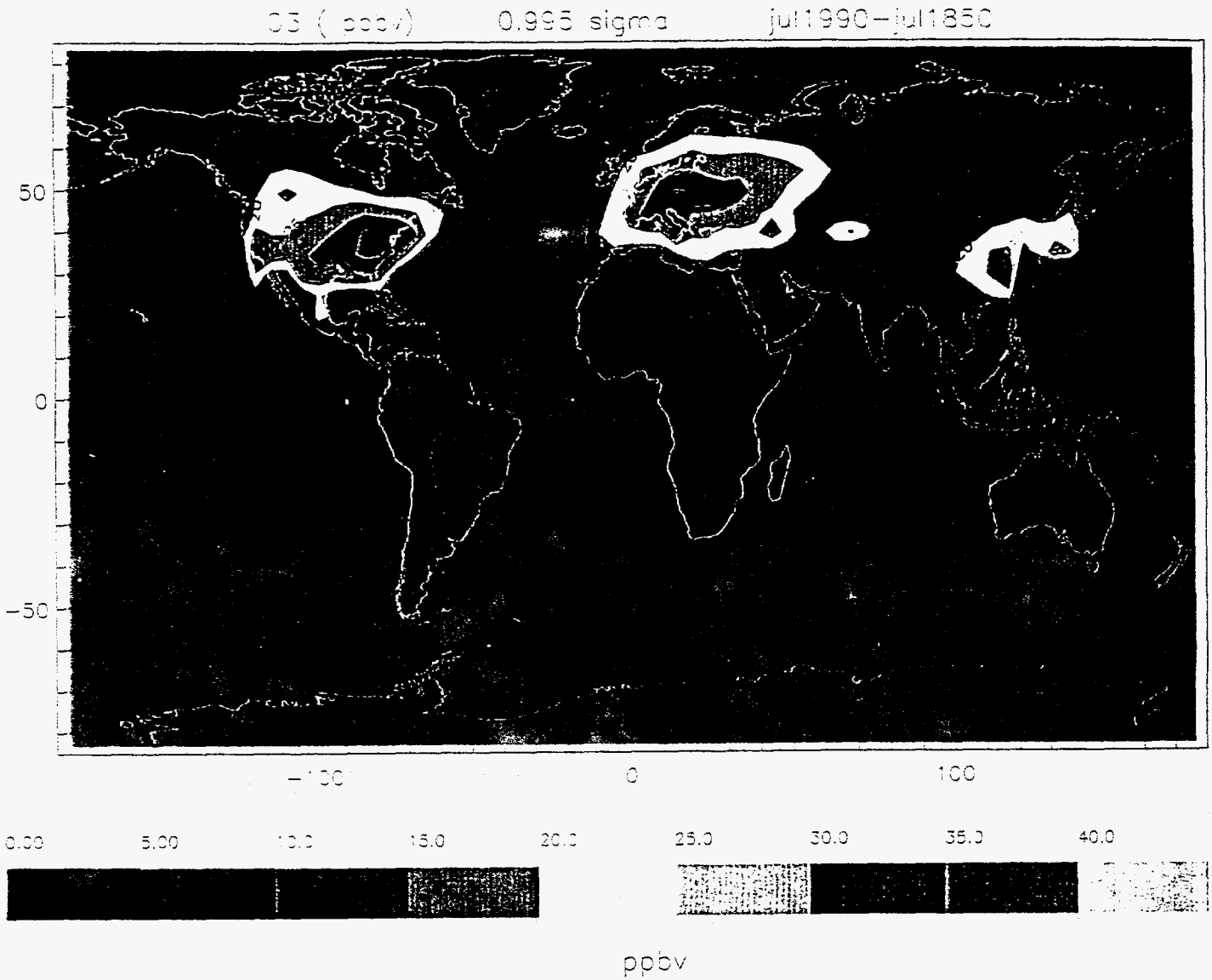

Figure 9, Changes in ozone concentration (%) between 1850 and 1990 in July at the surface level. The results suggest that the rapid industrial increase in the emission of NOx and CO leads to a significant ozone increase (more than 30ppbv or 150% in North America and in Europe). There is a also indication that the increase in biomas burning emissions in the tropics could have produced an important ozone increase.

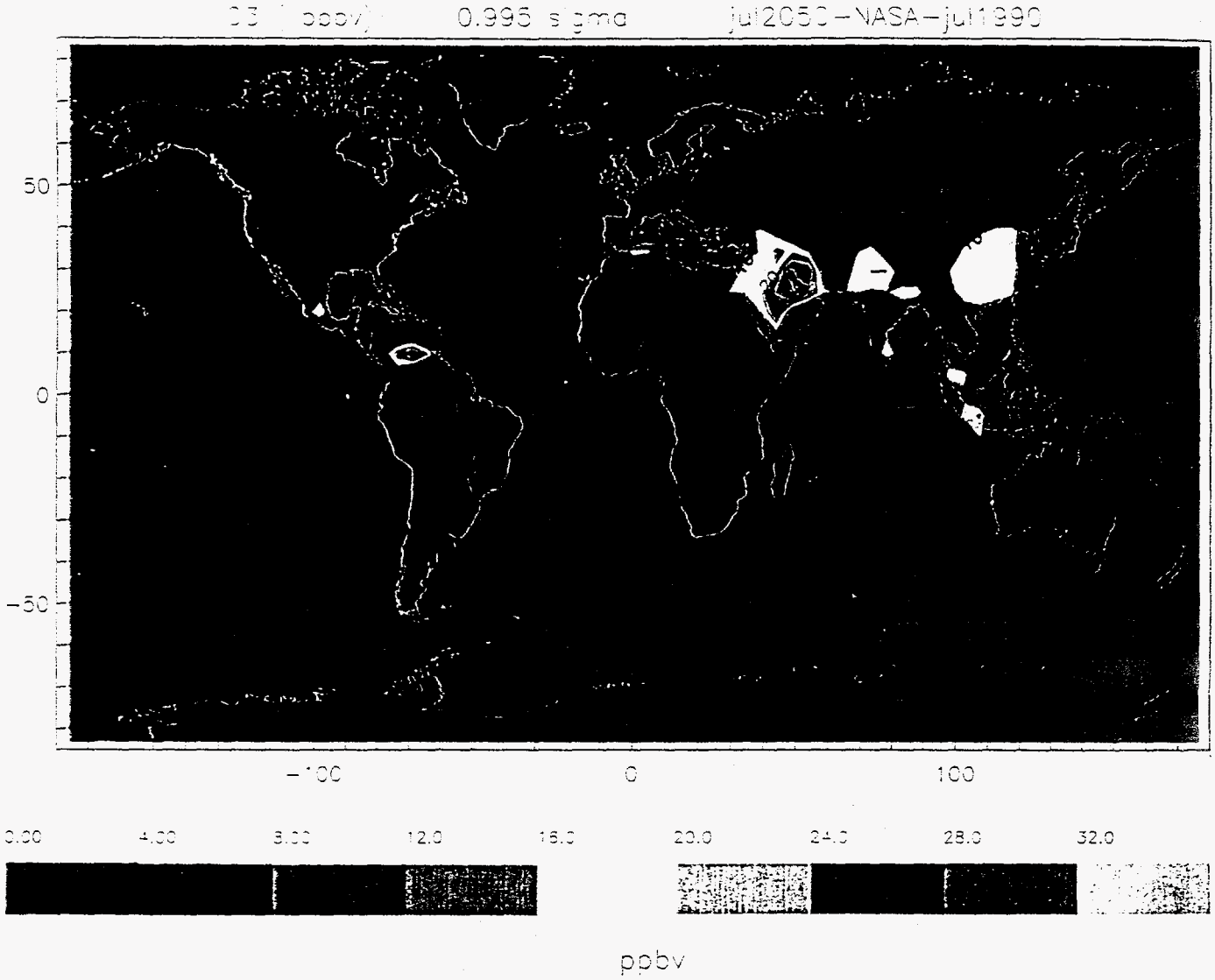

Figure 6, Predicted changes in the ozone concentration (ppbv) between 1990 and 2050 in July at the surface level. Future ozone increases are predicted to be highest in the countries where fuel consumption will rapidly increase in the future (such as China, India, and South-East Asia). The maximum increase in ozone is about 20 ppbv (approximately 30-70% increase).

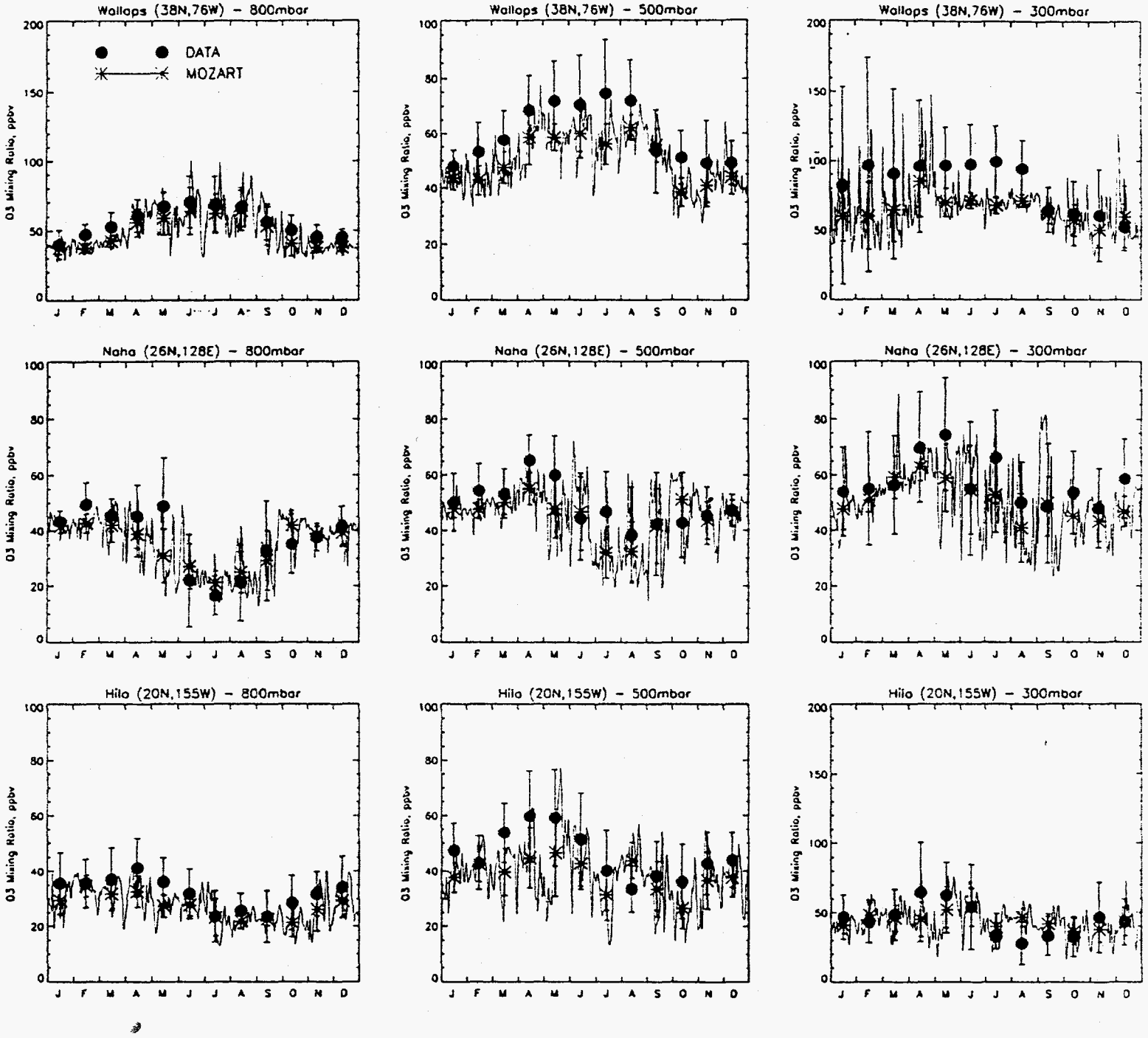

Figure 11 . Measured (full circles) and calculated (day-to-day, solid line; monthly mean, stars) seasonal cycle of O_3 mixing ratio (ppbv) at 12 stations and at 500 mb.